Journal of Medicinal Chemistry

Article

A2B Adenosine Receptor Antagonists with Picomolar Potency

Jie Jiang, Catharina Seel, Ahmed Temirak, Vigneshwaran Namasivayam, Antonella Arridu, Jakub Schabikowski, Younis Baqi, Sonja Hinz, Jörg Hockemeyer, and Christa E Müller

J. Med. Chem., **Just Accepted Manuscript** • DOI: 10.1021/acs.jmedchem.9b00071 • Publication Date (Web): 05 Mar 2019

ACS Publications

is published by the American Chemical Society. 1155 Sixteenth Street N.W., Washington, DC 20036

A_{2B} Adenosine Receptor Antagonists with Picomolar Potency

Jie Jiang,[1,&] Catharina Julia Seel,[1] Ahmed Temirak,[1] Vigneshwaran Namasivayam,[1] Antonella Arridu,[1] Jakub Schabikowski,[1,#] Younis Baqi,[2] Sonja Hinz,[1] Jörg Hockemeyer,[1] Christa E. Müller*[1]

[1]PharmaCenter Bonn, Pharmaceutical Institute, Pharmaceutical Chemistry I, An der Immenburg 4, D-53121 Bonn, Germany.

[2]Department of Chemistry, Faculty of Science, Sultan Qaboos University, PO Box 36, Postal Code 123, Muscat, Oman.

[&]Present address: Key Laboratory of Colloid and Interface Chemistry & Key Laboratory of Special Aggregated Materials, Shandong University, Ministry of Education, Jinan 250100, P. R. China

[#]J.S. was on leave from the Department of Technology and Biotechnology of Drugs, Faculty of Pharmacy, Jagiellonian University Medical College, Kraków, Poland

KEYWORDS

Adenosine, adenosine A_{2B} receptor, antagonist, cancer, halogen bonding, immunotherapy, molecular modeling, structure-activity relationships, sulfonamide synthesis, xanthine

ABSTRACT

The A_{2B} adenosine receptor (A_{2B}AR) was proposed as a novel target for the (immuno)therapy of cancer since A_{2B}AR blockade results in antiproliferative, anti-angiogenic, anti-metastatic, and immuno-stimulatory effects. In this study, we explored the structure-activity relationships of xanthin-8-yl-benzenesulfonamides mainly by introducing a variety of linkers and substituents attached to the sulfonamide residue. A new, convergent strategy was established which facilitated the synthesis of the target compounds. Many of the new compounds exhibited subnanomolar affinity for the A_{2B}AR combined with high selectivity. Functional groups were introduced which will allow the attachment of dyes and other reporter groups. 8-(4-((4-(4-Bromophenyl)piperazin-1-yl)sulfonyl)phenyl)-1-propylxanthine (**34**, PSB-1901) was the most potent A_{2B}-antagonist (K_i 0.0835 nM, K_B 0.0598 nM, human A_{2B}AR) with >10,000-fold selectivity versus all other AR subtypes. It was similarly potent and selective at the mouse A_{2B}AR, making it a promising tool for preclinical studies. Computational studies predicted halogen bonding to contribute to the outstanding potency of **34**.

INTRODUCTION

G protein-coupled receptors (GPCRs) are the largest family of transmembrane signaling proteins in the human genome and constitute the most important class of drug targets.[1, 2] Among the class A, rhodopsin-like GPCRs, adenosine-activated receptors (ARs) are an important subfamily, which is involved in a variety of physiological and pathological functions.[3, 4] Four subtypes of ARs exist which are termed A_1, A_{2A}, A_{2B} and A_3. The A_{2B}AR shows the lowest affinity for adenosine among all four subtypes.[2, 5] Thus, the A_{2B}AR is thought to remain silent under normal physiological conditions where extracellular adenosine levels range between 30 to 300 nM.[3] However, the receptor becomes activated under pathological conditions such as hypoxia, inflammation and cancer, where extracellular adenosine levels are increased up to micromolar concentrations.

While A_{2B}AR expression is ubiquitously found, typically at low levels, higher expression is detected in human cecum, large intestine, mast cells, and hematopoietic cells.[6] Importantly, A_{2B}AR expression can be upregulated by disease; significant upregulation is observed by hypoxia inducible factor 1-α (HIF-1α), in many cancers, and under inflammatory conditions.[7] Both, increase in extracellular adenosine concentrations,[8] and upregulation of A_{2B}AR expression under pathological conditions[9, 10] indicate an important role of the A_{2B}AR in disease. A_{2A} and A_{2B}ARs are the most closely related AR subtypes, which are frequently co-expressed on cells. We recently demonstrated the formation of heteromeric A_{2A}-A_{2B}AR complexes and revealed that ligand recognition and signaling of the A_{2A}AR is blocked by the A_{2B}AR, which leads to significantly altered pharmacology of A_{2A}ARs.[11]

A_{2B}AR antagonists have been proposed as drugs for the treatment of asthma, inflammation, pain, diabetes, and Alzheimer's disease.[12, 13] Recent findings further revealed that A_{2B}AR antagonists can directly influence the growth and migration of cancerous cells of bladder, breast, colon and

prostate.[14-17] In addition, adenosine was found to be favorable for cancerous cell survival due to its immuno-suppressive effects.[18, 19] Adenosine inhibits cytotoxic effector functions of natural killer and T cells mainly through A_{2A}AR signaling, which results in tumor immune escape and evasion. Preclinical studies have confirmed that the blockade of A_{2A}AR activation markedly promotes antitumor immunity.[20] On the other hand, adenosine polarizes myeloid cells to develop into immunosuppressive M2 macrophages and tolerogenic dendritic cells by A_{2A} and A_{2B}AR stimulation. There is growing evidence that tumor progression can also be delayed by A_{2B}AR blockade through inhibiting tumor myeloid-derived suppressor cell accumulation and by restoring efficient antitumor T cells.[21, 22] These results implicate that the A_{2B}AR acts as an important promoter of cancer growth and cancer immune evasion, and therefore antagonists of this receptor are regarded as promising new cancer (immuno)therapeutics, which not only activate the immune system, but, in addition display direct anti-proliferative effects, and, moreover, can reduce pain.[13]

The non-selective AR antagonists caffeine and theophylline, which block human A_1, A_{2A}, A_{2B} and A_3AR at micromolar concentrations, are used as central stimulants (caffeine), for the treatment of sleep apnoea and for improving lung functions in pre-term babies (caffeine), as anti-asthmatics (theophylline), and for the treatment of pain in combination with analgesics (caffeine). The analgesic effect of caffeine, and its synergism with paracetamol and non-steroidal anti-inflammatory drugs, are due to the blockade of A_{2B}ARs.[23] Moreover, caffeine has recently been shown to have anti-cancer effects in animal studies due to the blockade of both A_{2A} and A_{2B}AR.[24-26] Several epidemiological studies indicated that caffeine may protect humans from some cancer types, but other studies were not conclusive.[24, 27]

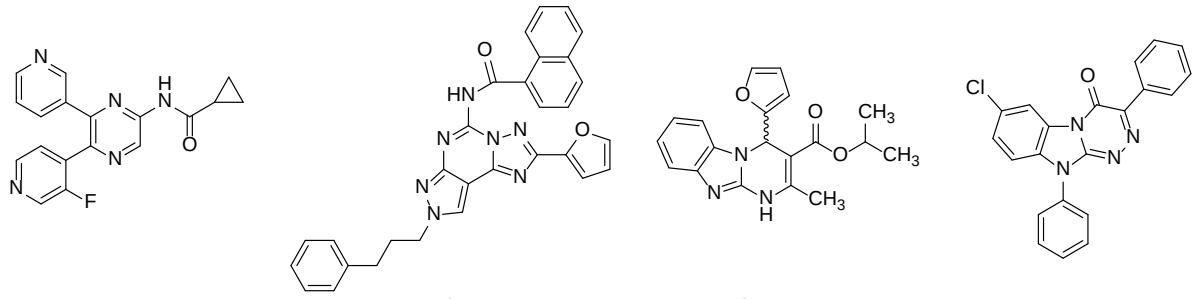

1 LAS101057

human	
A_{2B}	= 24 nM
A_{2A}	> 2500 nM
A_1	>10000 nM
A_3	>10000 nM

2

human	
A_{2B}	= 20 nM
A_{2A}	= 800 nM
A_1	= 1100 nM
A_3	= 300 nM

3 ISAM140

human	
A_{2B}	= 3.49 nM
A_{2A}	> 10000 nM
A_1	> 10000 nM
A_3	> 10000 nM

4

human	
A_{2B}	= 3.10 nM
A_{2A}	> 10000 nM
A_1	> 10000 nM
A_3	> 1000 nM

Figure 1. Structures and K_i values of known non-xanthine A_{2B}AR antagonists.[28-31]

Considerable efforts have been made in recent years to develop selective high-affinity antagonists for A_{2B}ARs. These compounds can be divided into non-xanthine derivatives (Fig. 1), for example 2-aminopyrazines (e.g. **1**),[28] pyrazolotriazolopyrimidines (e.g. **2**),[29] pyrimidobenzimidazoles (e.g. **3**),[30] triazinobenzimidazolones (e.g. **4**),[31] and xanthine derivatives related to the natural products caffeine and theophylline (Fig. 2).

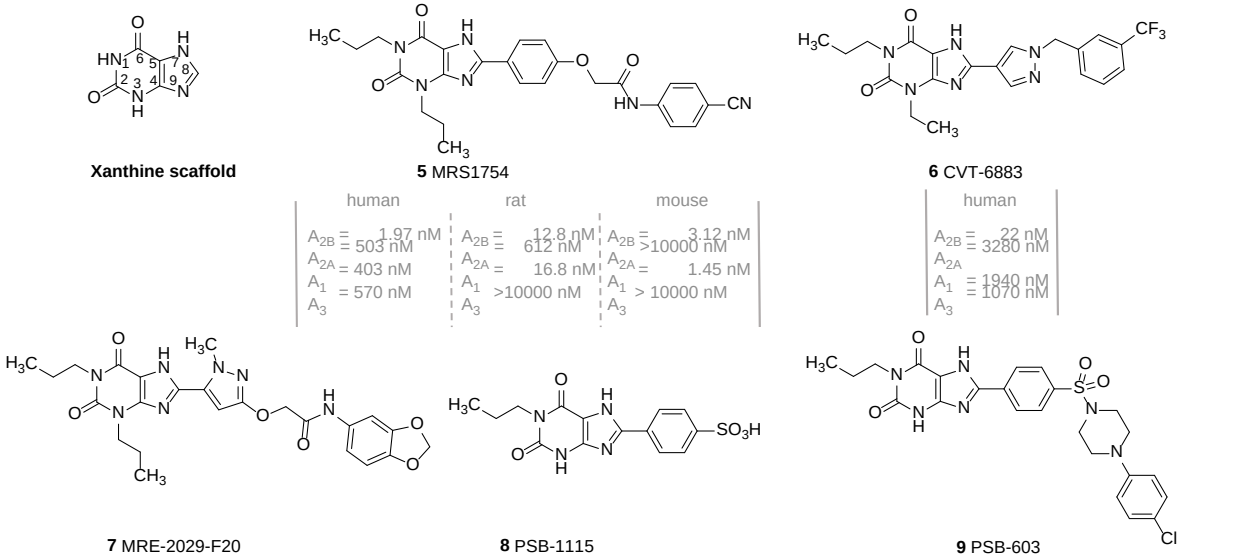

Xanthine scaffold

5 MRS1754

human		rat		mouse	
A_{2B}	= 1.97 nM	A_{2B}	= 12.8 nM	A_{2B}	= 3.12 nM
A_{2B}	= 503 nM	A_{2B}	= 612 nM	A_{2B}	>10000 nM
A_{2A}	= 403 nM	A_{2A}	= 16.8 nM	A_{2A}	= 1.45 nM
A_1	= 570 nM	A_1	>10000 nM	A_1	> 10000 nM
A_3		A_3		A_3	

6 CVT-6883

human	
A_{2B}	= 22 nM
A_{2B}	= 3280 nM
A_{2A}	
A_1	= 1940 nM
A_3	= 1070 nM

7 MRE-2029-F20

human	
A_{2B}	= 5.5 nM
A_{2A}	>1000 nM
A_1	= 200 nM
A_3	>1000 nM

8 PSB-1115

human		rat		mouse	
A_{2B}	= 53.4 nM	A_{2B}	= 3140 nM	A_{2B}	= 1940 nM
A_{2B}	= 3790 nM	A_{2B}	= 24000 nM	A_{2B}	>10000 nM
A_{2A}		A_{2A}		A_{2A}	= 591 nM
A_1	>10000 nM	A_1	= 2200 nM	A_1	>10000 nM
A_3	>10000 nM	A_3	> 10000 nM	A_3	

9 PSB-603

human		rat		mouse	
A_{2B}	= 0.553 nM	A_{2B}	= 0.355 nM	A_{2B}	= 0.265 nM
A_{2B}	> 10000 nM	A_{2B}	> 10000 nM	A_{2B}	>10000 nM
A_{2A}		A_{2A}		A_{2A}	= 42.4 nM
A_1	> 10000 nM	A_1	> 10000 nM	A_1	>10000 nM
A_3	> 10000 nM	A_3	> 10000 nM	A_3	

Figure 2. Selected xanthine-based A_{2B}ARs antagonists and their K_i values at AR subtypes.[2, 32]

Some selected xanthine-based A_{2B}AR antagonists are shown in Figure 2, e.g. MRS1754 (**5**)[33], CVT-6883 (GS6201, **6**),[34] MRE2029-F20 (**7**),[35] PSB-1115 (**8**),[36] and PSB-603 (**9**)[37]. Compound **5** was the first potent, A_{2B}AR-selective antagonist, for which a Th1-suppressive effect in autoimmune diseases was shown.[38] It significantly inhibited colon carcinoma cell growth in a dose-dependent manner, and induced anti-angiogenesis in microvascular endothelial cells.[39, 40] Compound **6** was clinically evaluated in a phase I trial with the aim to develop it as a drug for the treatment of lung remodeling, pulmonary hypertension and asthma.[2, 34, 41, 42] Further studies found that **6** led to a more favorable cardiac remodeling and reduced ventricular dysfunction and ventricular arrhythmias after acute myocardial infarction in the mouse or rat.[43, 44]

Our group has been interested in improving the potency, selectivity and/or water-solubility of xanthine-based A_{2B}AR antagonists, and a series of sulfonic acid and sulfonamide derivatives has previously been developed. For example, the water-soluble sulfophenylxanthine derivate **8** (PSB-1115) is a selective A_{2B}AR antagonist in humans, that displayed dose-dependent antinociceptive effects and could potently diminish inflammatory pain in mice, showing synergism with other analgesics including morphine, non-steroidal anti-inflammatory drugs, and pegylated adenosine deaminase (PEG-ADA, an FDA approved drug).[23, 45, 46] Recent research further revealed that **8** improved intestinal barrier function in colon inflammation, and under hypoxic/ischemic conditions and reperfusion injury.[47] In addition, **8** reduced the immuno-suppression in a tumor environment and inhibited tumor angiogenesis with increasing T cells numbers in a mouse melanoma model.[13, 21, 48]The sulfonate function of **8** confers high water-solubility, however, the deprotonation of this free sulfonic acid group under physiological conditions ($pK_a < 1$) likely prevents peroral absorption and central nervous system (CNS) penetration.

A sulfonamide group was introduced instead to solve the drawbacks of the sulfonate moiety. Compound **9** (PSB-603) was then developed as one of the most potent and selective A_{2B}AR antagonists in all three species, human, rat, and mouse.[32, 37] Compound **9** was found to inhibit the growth of prostate cancer cells and to attenuate cell proliferation of neuroendocrine tumours.[7, 15, 49] Compound **8** and **9** were also found to be useful for treating infectious diseases due to their immunostimulatory effects, and to prevent A_{2B}AR-induced opening of the blood-brain barrier.[50, 51] All of these findings confirmed that A_{2B}AR antagonists have a great potential as future drugs and are particularly promising for the immunotherapy of cancer and infectious diseases.

A tritium-labeled derivative of **9**, [^{3}H]PSB-603, has been prepared, and a radioligand binding assay was established for the labeling of A_{2B}ARs.[1, 37] Recently, the first potent and selective fluorescent A_{2B}AR ligands were reported.[52]

Homology modeling based on the X-ray structures of the related A_{2A}AR and site-directed mutagenesis studies have provided fundamental information of the A_{2B}AR and its orthosteric binding site.On the basis of the most potent A_{2B}AR antagonist, compound **9**, we established a pharmacophore model (Fig. 3), in which the xanthine scaffold represents a flat core, that offers a hydrogen bond acceptor (the C6-carbonyl function) - hydrogen bond donor (N7-hydrogen) motif. A benzenesulfonamide spacer, which features hydrogen bond acceptor groups, was used to connect the flat core with another aromatic residue. Propyl substitution at position 1 was optimal and found to increase A_{2B}AR affinity via hydrophobic interactions with the amino acid residue Trp247$^{6.48}$. A free NH at position 3 enhanced potency at the A_{2B}AR as well as selectivity versus the A_1, A_{2A}, and A_3AR subtypes. The hydrophobic interactions between Val250$^{6.51}$ and the xanthine core, as well as Leu81$^{3.28}$ and the aromatic ring that is connected to the xanthine core, appear to be crucial for high A_{2B}AR binding affinity of antagonist **9** [36, 55, 56] However, interactions of the sulfonamide

residue have not been clearly elucidated so far. In the present study, we varied the spacers and the substituted aromatic ring attached to the xanthine-8-phenylsulfonate via sulfonamide formation. Our aim was (i) to explore the structure-activity relationships (SARs) for obtaining highly potent and selective A_{2B}AR antagonists, (ii) to modulate the compounds' physicochemical properties, (iii) to develop ligands for potential further labeling with fluorescent dyes or other reporter groups, and (iv) to explore the possibility of obtaining dual A_{2A}/A_{2B} AR antagonists. Computational studies were performed to rationalize the SARs for these sulfonamidophenyl-xanthine derivatives.

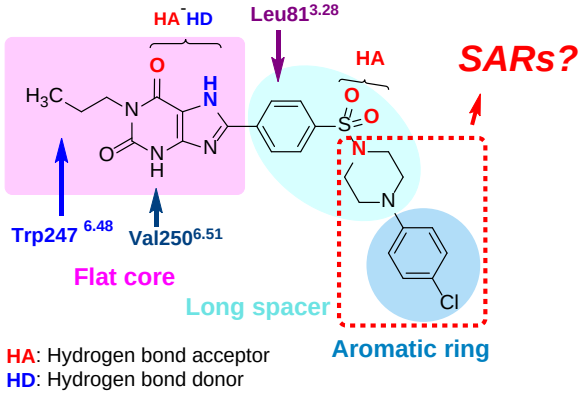

Figure 3. Features of A_{2B}AR antagonist **9** that are important for binding to the receptor.

RESULTS and DISCUSSION

Chemistry. The synthetic routes for the target compounds are described in Scheme 1 and 2. 3-Propyl-substituted 5,6-diaminouracil derivatives **10a-c** were obtained according to previously reported procedures.[57-59] Detailed synthetic information for compound **11** and some of the required amines (**58**, **60**, **62-64**, **81**, **82**, **85-87** and **89**) is provided in the Supporting Information.[36] Compounds **10a-c** and **11** were subsequently condensed in the presence of *N*-(3-(dimethylamino)propyl)-*N*′-ethylcarbodiimide (EDC) to yield amides **12a-c** (see Scheme 1). After ring closure of **12a-c** using various condensation methods (see Scheme 1) yielding xanthines **13a-**

c, different piperazine derivatives (**55-84** and **88-90**) or other amines (**91**, **92**) were introduced to obtain the corresponding xanthine sulfonamide derivatives **14-44** and **50-54** (see Scheme 1). Aminolysis was performed using optimized conditions in dry dimethyl sulfoxide (DMSO) under an argon atmosphere, instead of dimethylformamide (DMF) which had been used before.[37] Dry DMSO prevented ester hydrolysis observed in the presence of water, as well as side-reactions with dimethylamine which resulted from DMF decomposition yielding compound **53**. In this modified nucleophilic substitution reaction, pure sulfonamide products were obtained for reactions of acyclic amines **91** and **92** yielding **53** and **54**, while side-products were obtained for sterically hindered piperazine derivatives. These resulted from the competing pathway by attack at the electron-deficient carbon atom of the nitro phenyl ester.

A new synthetic route was designed for the preparation of some of the final products as depicted in Scheme 2. The sulfonamide-substituted benzoic acid derivatives **85b-87b** were prepared from piperazine derivatives **85-87** and 4-(chlorosulfonyl)benzoic acid (**11a**), and subsequently coupled with **10a** yielding **85c-87c**. The final ring closure reaction was performed with P_2O_5 for 10 min to yield xanthines **45-47**. The methoxyphenyl derivatives **46** and **47** were further subjected to demethylation to furnish the phenol derivatives **48** and **49**. This new method to prepare the targeted xanthine derivatives was found to be more economic and convenient compared with the previously described procedure.

The final products were purified by reversed-phase high performance liquid chromatography (RP-HPLC) or directly recrystallized from acetonitrile. Newly synthesized xanthine-8-yl-benzenesulfonamides are listed in Table 1. All products were characterized by ^{1}H and ^{13}C NMR spectroscopy as well as mass spectrometry (MS) employing electrospray ionization (ESI).

Scheme 1. Preparation of sulfonamides **14-44** and **50-54**.[a,b]

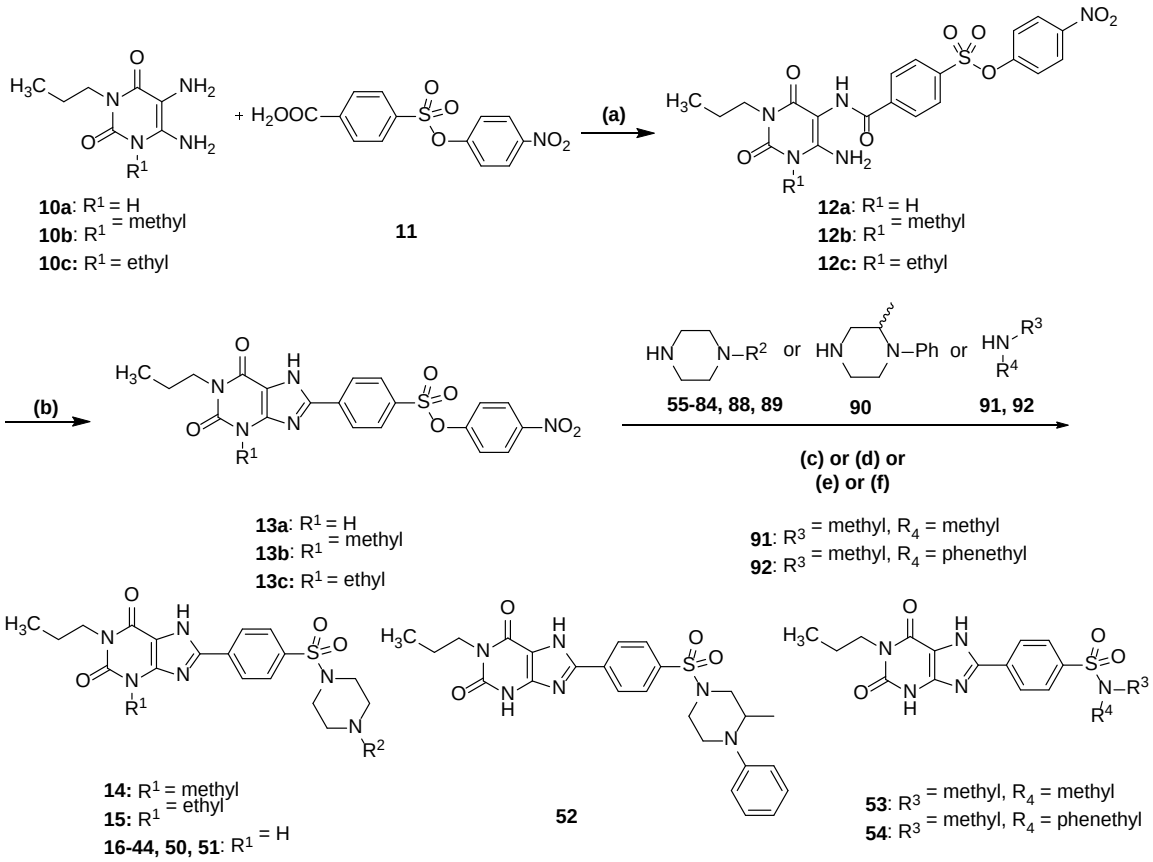

[a] Reagents and conditions: (a) EDC, MeOH, rt, 4 h; (b) polyphosphoric acid trimethylsilyl ester (PPSE), 170 °C, 5 h; (c) method A: DMF; (d) method B: dry DMSO, Ar, 3h, 150 °C; (e) method C: analogous to method A with consecutive reaction; (f) method D: dimethylamine in 33 % ethanolic solution, rt, 16h. [b] For R^2 see Table 1.

Scheme 2. New strategy for the preparation of compounds **45-49**.

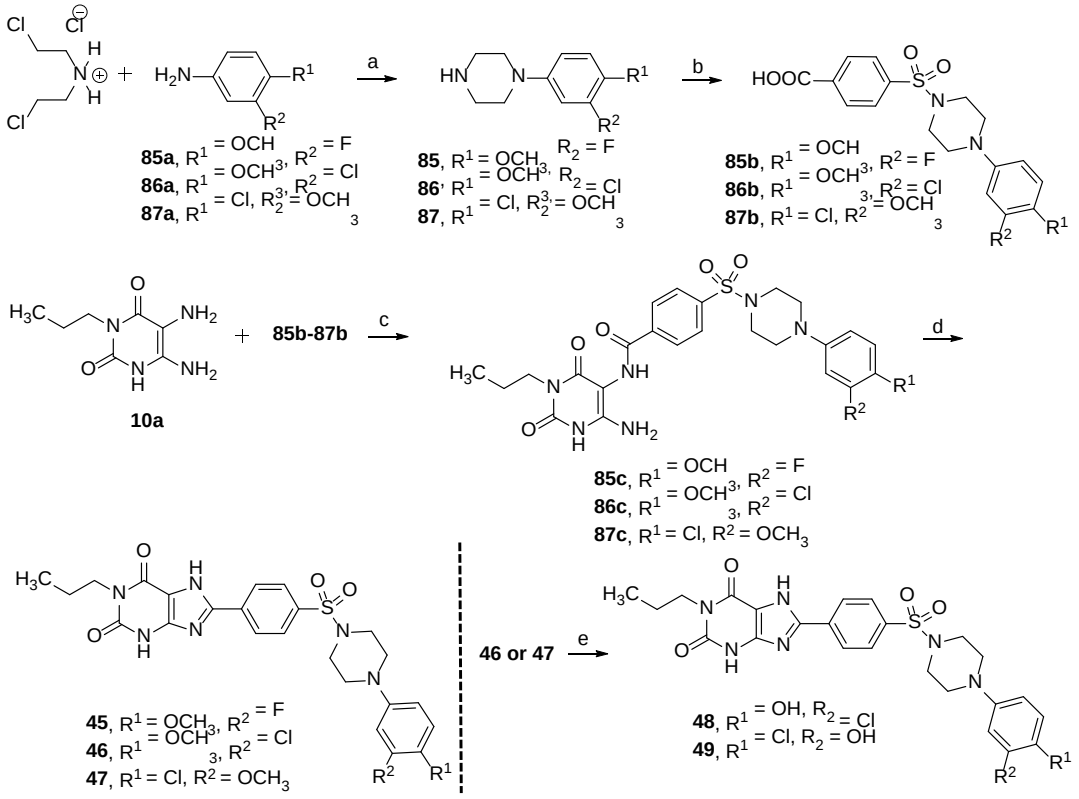

Reagents and conditions: (a) diethyleneglycol monomethylether, 150 °C, 20 h, 47-62 %; (b) 4-(chlorosulfonyl)benzoic acid (**11a**), *N*,*N*-diisopropylethylamine (DIPEA), dichloromethane (DCM), rt, 36 h, 72-87 %; (c) EDC*HCl, DMF, rt, 18 h, 50-90 %; (d) P_2O_5, DMF, reflux, 10 min, 10-58 %; (e) 1M BBr_3, DCM, rt, 24 h, 13-25 %.

Table 1. Isolated yields, purities and calculated physicochemical properties of newly synthesized sulfonamidophenylxanthine derivatives.

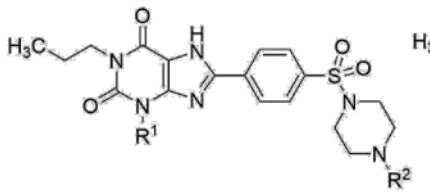

14: R^1 = Methyl; **15**: R^1 = Ethyl;
16-51: R^1 = H

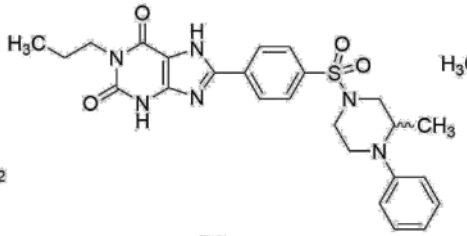

52

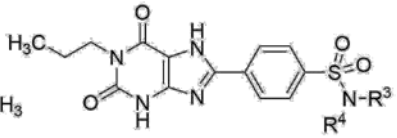

53, 54

Compd.[a]		Purity (%) [b]	M.W. [c]	Clog *P* [d]	PSA [d]
Piperazine derivatives					
14	**R²** = 4-chlorophenyl	98.1	543.0	3.5	109.9
15	**R²** = 4-chlorophenyl	97.4	557.1	3.9	109.9
16	**R²** = 4-bromobenzyl	98.8	587.5	4.3	118.7
17	**R²** = 3-bromobenzyl	100.0	587.5	4.3	118.7
18	**R²** = 3-methoxybenzyl	97.3	538.6	3.1	127.9
19	**R²** = 3-methylbenzyl	98.6	522.6	3.8	118.7
20 [e]	**R²** = 4-azidobenzyl	99.0	549.6	4.0	148.1
21 [f]	**R²** = benzyl-4-carboxylate	98.0	552.6	1.2	156.0
22	**R²** = 4-(2-hydroxyethoxy)benzyl	97.6	582.7	2.5	148.2
23	**R²** = 4-(2-(2-methoxyethoxy)ethoxybenzyl	95.1	626.7	3.1	146.4
24	**R²** = 3-fluoro-4-methoxybenzyl	97.8	556.6	3.4	127.9
25	**R²** = 4-fluoro-3-methoxybenzyl	98.5	556.6	3.4	127.9
26	**R²** = 3-fluoro-5-methoxybenzyl	100.0	556.6	3.4	127.9
27	**R²** = 3-fluoro-4-bromobenzyl	98.0	605.5	4.5	118.7
28	**R²** = phenyl	95.6	494.6	3.7	118.7
29	**R²** = 4-fluorophenyl	98.3	512.6	3.9	118.7
30	**R²** = 3-fluorophenyl	95.5	512.6	3.9	118.7
31	**R²** = 2-fluorophenyl	97.1	512.6	3.9	118.7

32 [g]	**R²** = 3-chlorophenyl	98.2	529.0	4.3	118.7
33 [g]	**R²** = 2- chlorophenyl	95.2	529.0	4.3	118.7
34	**R²** = 4-bromophenyl	99.1	573.5	4.5	118.7
35	**R²** = 3-bromophenyl	98.3	573.5	4.5	118.7
36	**R²** = 2-bromophenyl	97.8	573.5	4.5	118.7
37	**R²** = 4-iodophenyl	100.0	620.5	4.6	118.7
38	**R²** = 3-methoxyphenyl	97.6	524.6	3.6	127.9
39	**R²** = 4-methylphenyl	98.1	508.6	4.2	118.7
40	**R²** = 2-methylphenyl	98.5	508.6	4.2	118.7
41 [e]	**R²** = 4-hydroxyphenyl	98.4	510.6	3.4	138.9
42	**R²** = benzoyl	98.0	522.6	2.9	135.8
43	**R²** = 1-phenylethyl	95.8	522.6	3.7	118.7
44	**R²** = methyl	99.1	432.5	1.6	118.7
45 [g,]	**R²** = 3-fluoro-4-methoxyphenyl	95.8	542.6	3.7	127.9
46 [g]	**R²** = 3-chloro-4-methoxyphenyl	96.6	559.0	4.2	127.9
47 [g]	**R²** = 4-chloro-3-methoxyphenyl	96.6	559.0	4.2	127.9
48 [g]	**R²** = 3-chloro-4-hydroxyphenyl	99.0	545.0	4.0	138.9
49 [g]	**R²** = 4-chloro-3-hydroxyphenyl	95.0	545.0	4.0	138.9
50	**R²** = 4-chloro-2-fluorophenyl	97.4	547.0	4.5	118.7
51	**R²** = 4-(2-hydroxy-ethoxy)phenyl	98.4	554.6	2.9	148.2
52	*See structure above*	95.9	508.6	3.4	118.7
Acyclic amino derivatives					
53 [h]	**R³** = methyl **R⁴** = methyl	95.9	377.4	2.0	115.5
54	**R³** = methyl **R⁴** = phenethyl	99.1	467.5	4.0	115.5

[a] All final products were synthesized according to method B (see Scheme 1) unless otherwise noted. [b] Purity was determined by HPLC-UV-MS at 254 nm; [c] molecular weight was calculated by the Chemdraw software; [d] cLog*P* and polar surface area were calculated by ChemAxon;[e] synthesized

according to method A ; [f] synthesized according to method C. [g] synthesized according to method D; [h] synthesized according to method E.

Calculation of Physicochemical Properties and Solubility Determination of Selected Products

Several physicochemical parameters were calculated to estimate the potential suitability of the final products as tool compounds or drugs, including polar surface area (PSA) and lipophilicity (clog *P* value). PSA values were in all cases, except for compounds **20**-**23**, and **51**, lower than 140 Å^2, indicating that they might be intestinally absorbable.[60] All of the compounds showed a clog *P* value lower than 5, which is consistent with Lipinski's rule for drugs exhibiting pharmacokinetic properties that are suitable for peroral application.[61] Benzylpiperazine derivatives showed lower clog *P* values but the same PSA values as the corresponding phenylpiperazine derivatives (compare compounds **16**/**34**, **18**/**38**, and **19**/**39**). Compounds **14** and **15** which are substituted at the xanthine N3-position and therefore lack the corresponding hydrogen bond donor function display lower PSA values; modification at this position may allow modulation of the physicochemical parameters of the compounds. It should be kept in mind that these values were not experimentally determined and therefore provide only estimations. The water-solubility of *p*-chlorophenylpiperazine derivative **9** was determined in comparison to that of the analogous *p*-chlorobenzylpiperazine derivative **98** using a shaking flask method. The latter compound, which is more basic, displayed significantly higher solubility (3.2 μM) compared to **9** (0.2 μM). However, the solubility of the compounds should be further improved for use as therapeutics.

Biological Evaluation

Radioligand binding assays were performed to determine the affinities of the products at human and/or mouse A_1, A_{2A}, A_{2B}, and A_3AR subtypes. Human and mouse adenosine receptors recombinantly expressed in Chinese hamster ovary (CHO) cells or human embryonic kidney (HEK) cells were employed. The following radioligands were employed: [^{3}H]2-chloro-N^6-cyclopentyladenosine ([^{3}H]CCPA), [^{3}H](*E*)-3-(3-hydroxypropyl)-8-(2-(*m*-methoxyphenyl)vinyl)-7-methyl-1-prop-2-ynyl-3,7-dihydropurine-2,6-dione ([^{3}H]MSX-2), [^{3}H]8-(4-(4-(4-chlorophenyl)piperazine-1-sulfonyl)phenyl)-1-propyl-3,7-dihydropurine-2,6-dione ([^{3}H]PSB-

603), and [^{3}H]2-phenyl-8-ethyl-4-methyl-(8*R*)-4,5,7,8-tetrahydro-1*H*-imidazo[2.1-*i*]purin-5-one ([^{3}H]PSB-11) for human and mouse A_1, A_{2A}, A_{2B}, and human A_3AR. [^{3}H]5'-*N*-Ethylcarboxamidoadenosine ([^{3}H]NECA) was used as a radioligand for assays at the mouse A_3AR due to the low potency of [^{3}H]PSB-11 at the rodent receptors. Biological data for human ARs are summarized in Tables 2−6 and Figure 4−7. Selected data of published compounds are included for comparison. Concentration-inhibition curves of selected compounds are depicted in Figure 8. These compounds were further explored at the mouse AR subtypes to investigate potential species differences. In addition, for selected compounds cAMP accumulation assays were performed in recombinant A_{2B}AR-expressing CHO cells to demonstrate their functional properties as antagonists (see below).

Structure-Activity Relationships

The previously developed sulfonate **8** exhibits high water-solubility and has been used in in vivo studies; however, its A_{2B}AR affinity is moderate, its selectivity, especially in rodents, is low, and it is too polar for oral absorption.[32, 36, 55] A prodrug concept had been developed to overcome the latter issue. [36] Later on, sulfonamide derivatives of **8**, such as xanthine **9**, were synthesized.[37] Although A_{2B}AR affinity and selectivity of **9** are already high, a broad exploration of the SARs of this class of compounds is required. This will provide highly useful knowledge allowing to fine-tune the compounds' properties in subsequent multi-dimensional drug development efforts. Moreover, comprehensive exploration of SARs is needed as a basis for molecular modeling studies to explore the ligand binding site, since X-ray structures of the A_{2B}AR are still lacking. Therefore, taking compounds **8** and **9** as lead structures, a variety of 8-phenylxanthine derivatives bearing a broad range of *p*-sulfonamido-substituents was synthesized in this study and optimized as A_{2B}AR antagonists. Most of the investigated compounds showed high affinity for the A_{2B}AR with K_i values

in the nanomolar or even subnanomolar range, very high selectivity versus A_1 and A_3ARs, and different degrees of selectivity towards the A_{2A}AR.

Table 2. Adenosine receptors affinities of *N*3-substituted compounds compared with PSB-603.

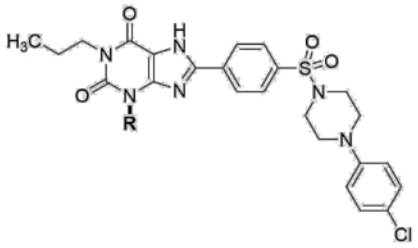

Compd.	R	K_i ± SEM (nM) (or % inhibition of radioligand binding at indicated concentration)				Selectivity Index[e]
		human A_{2B}[a]	human A_{2A}[b]	human A_1[c]	human A_3[d]	
9 PSB-603 [37]	H	**0.553**	>10000	>10000	>10000	>18000
14	Methyl	**1.91** ± 0.32	>1000 (33)[f]	>1000 (22)[f]	>1000 (39)[f]	>520
15	Ethyl	**4.31** ± 1.16	322 ± 157	>1000 (24)[f]	>1000 (28)[f]	75

[a] vs. [^{3}H]PSB-603 (n = 3); [b] vs. [^{3}H]MSX-2 (n = 3); [c] vs. [^{3}H]CCPA (n = 3); [d] vs. [^{3}H]PSB-11 (n = 3); [e] selectivity index was calculated by dividing the second lowest K_i value by the A_{2B}AR K_i value; [f] percent inhibition of radioligand binding at 1 μM.

In our previous study, 1-propyl substitution had been proven to be optimal conferring high A_{2B}AR affinity combined with high selectivity versus all other AR subtypes (see compound **9**, Figure 2). [37] A free NH function at position 7 is known to be crucial as a hydrogen bond donor for interacting with the A_{2B}AR and to allow the 8-phenyl ring to be coplanar with the xanthine core structure. [13] Even though 3-substituted compounds are not preferred based on previous results, we introduced small residues, methyl and ethyl, to potentially modulate the physicochemical properties of the xanthine derivatives by removing the N3-H donor function. The rank order of A_{2B}AR affinities for these compounds was as follows: H (**9**, 0.553 nM) > methyl (**14**, 1.91 nM, p = 0.0157 *) ≥ ethyl

(**15**, 4.31 nM). The selectivity was also decreased in the same order. But affinity and selectivity (**14**, >524-fold selective; **15**, ≥75-fold) of both *N*3-substituted xanthine derivatives were still high enough for potential application as A_{2B}-selective drugs (see Table 2). Nevertheless, compound **15** also displayed significant affinity for the A_{2A}AR indicating that the development of dual A_{2A}/A_{2B} antagonists via substitution of the *N*3-position would be feasible. Furthermore, the increased lipophilicity might increase the chances for brain penetration.

Table 3. Adenosine receptor affinities of 8-sulfonamidoxanthines with variations of residues on the sulfonamido function.

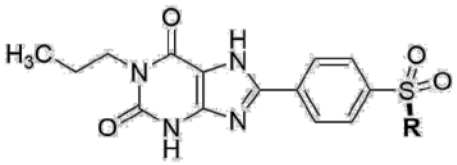

Compd.	R	K_i ± SEM (nM) (or % inhibition of radioligand binding at indicated concentration				Selectivity Index[e]
		human A_{2B}[a]	human A_{2A}[b]	human A_1[c]	human A_3[d]	
28	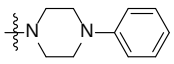	**0.643** ± 0.035	122 ± 32[f]	364 ± 57[f]	>1000 (27%)[g]	190
44	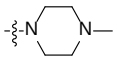	**48.2** ± 10.9[f]	140 ± 91	334 ± 109[f]	>1000 (7%)[g]	3
53		**18.6** ± 0.9	52.7 ± 12.2	190 ± 54[f]	1220 ± 220	3
54	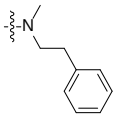	**1.69** ± 0.73[f]	357 ± 75[f]	1036 ± 384[f]	>1000 (4%)[g]	210
93[56]	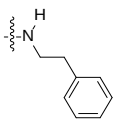	**3.62**	769	183	≥10000	50

[a] vs. [^{3}H]PSB-603 (n = 3); [b] vs. [^{3}H]MSX-2 (n = 3); [c] vs. [^{3}H]CCPA (n = 3); [d] vs. [^{3}H]PSB-11 (n = 3); [e] selectivity index was calculated by dividing the second lowest K_i value by the A_{2B}AR K_i value; [f] extrapolated curve; [g] percent inhibition of radioligand binding at 1 μM.

Our main focus was the introduction of a variety of substituents on the sulfonamido function. Removal of the *para*-chloro substituent in lead structure **9** (Fig. 2) resulted in **28**, which showed similar potency, but lower selectivity. Replacing the terminal phenyl ring of **28** by a methyl group (in **44**) strongly reduced A_{2B} affinity (by 76-fold) without much change at the other AR subtypes. Replacement of the piperazine ring by the small dimethylamine (in **53**) yielded a potent A_{2B} antagonist (K_i 18.6 nM), that showed, however, only moderate selectivity especially versus A_{2A} (3-fold) and A_1 (10-fold) receptors. Introducing a larger phenethyl residue (**93**) increased potency again (K_i 3.62 nM) as well as selectivity. Additional *N*-methylation leading to **54** retained A_{2B}AR affinity and increased selectivity, particularly versus the A_1AR subtype. These data indicated that an aromatic residue was favorable for high A_{2B}AR affinity and also for selectivity (compare **28**/**44**, p = 0.0021**, and **53**/**54**, p < 0.0001 ***). Moreover, disubstitution of the sulfonamide *N*-atom appears to contribute to high A_{2B}AR selectivity, and a piperazine residue is advantageous. Based on these findings, we concentrated our efforts on piperazine derivatives containing a terminal aromatic residue, and a large series of piperazine derivatives was designed and synthesized (Figure 4). SARs were further explored regarding the following aspects: (i) the type of linker between the piperazine and the aromatic ring; (ii) substitution of the aromatic ring (type of substituent, position, mono- and di-substitution, and functional groups for further attachment of moieties, e.g. for future fluorescent labeling).

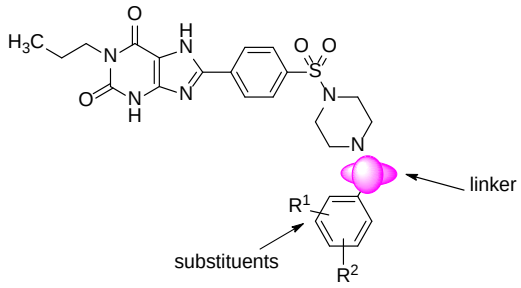

Figure 4. Structures of targeted piperazinyl-substituted sulfonamide derivatives.

Linker modification

A methylene or an ethylene group between the piperazine ring and the aromatic residue of the phenylpiperazine derivative **28**, was previously found to be tolerated (see benzylpiperazine **94** and phenethylpiperazine **95**).[55] However, the phenylpiperazine was 6-fold more potent than the corresponding benzylpiperazine derivative (compare **28**/**94**, K_i 0.634 nM vs. 3.6 nM) and 12-fold more potent than the phenethyl derivative **95** (K_i 7.51 nM). The rank order of A_{2B}AR affinities and selectivities vs. A_{2A}ARs among compounds with different linker length, i.e. number of CH_2 groups, was as follows: $(CH_2)_0$ (**28**, 0.643 nM, 190-fold vs. A_{2A}AR) > $(CH_2)_1$ (**94**, 3.6 nM, 134-fold vs. A_{2A}AR, p = 0.0002 ***) > $(CH_2)_2$ (**95**, 7.51 nM, 36-fold vs. A_{2A}AR, p = 0.0228 *), indicating that A_{2B}AR potency improved with decreasing linker length of the alkyl chain between the piperazine residue and the aromatic ring.

As alternative linkers carbonyl (**42**, K_i 5.69 nM), and methylbenzyl (**43**, K_i 8.34 nM) were explored, both of which were tolerated, but also resulted in decreased potency compared to **28**. In compound **52**, the phenyl ring was attached to the 3-position of the piperazine ring combined with *N*-methylation. This modification was also tolerated (K_i 7.15 nM) showing again that an aromatic ring increases potency (compare **44** (without phenyl substitution)/**52**), but it was 11-fold less potent than benzylpiperazine derivative **28**.

Direct attachment of the phenyl ring to the piperazine *N*-atom resulted in the highest A_{2B} affinity (sub-nanomolar K_i value) combined with the highest selectivity index. However, modulation is possible and may be used for the future fine-tuning. Especially a benzyl or a 1-methylbenzyl residue (compounds **94** and **43**) still yield potent and selective A_{2B}AR antagonists which feature increased basicity as compared to the aniline derivative **28** and might therefore display somewhat increased solubility. On the other hand, a carbonyl linker as in benzoylpiperazine **42**, resulted in increased A_{2A}AR affinity (K_i A_{2A} 143 nM, K_i A_{2B} 5.69 nM), still with a 30-fold selectivity for the A_{2B}AR, but this class of compounds may be suitable for future optimization aimed at obtaining dual A_{2A}/A_{2B} antagonists.

Table 4. Adenosine receptors affinities of xanthine-8-yl-benzenesulfonamide derivatives with linker modification.

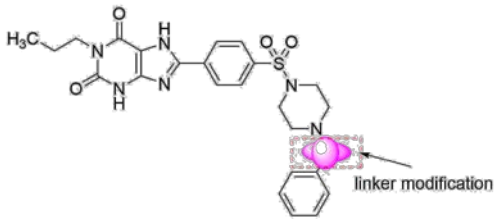

Compd.	Linker	K_i ± SEM (nM) (or % inhibition of radio ligand binding at indicated concentration)				Selectivity Index[e]
		human A_{2B}[a]	human A_{2A}[b]	human A_1[c]	human A_3[d]	
28	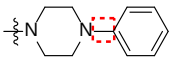	**0.643** ± 0.035	122 ± 32[f]	364 ± 57[f]	>1000 (27%)[g]	190
42	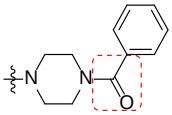	**5.69** ± 0.35	143 ± 18[f]	>1000 (15%)[g]	>1000 (26%)[g]	30

43	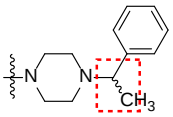	**8.34** ± 1.51	≥1000 (42)[g]	≥1000 (42%)[g]	>1000 (0)[g]	>120
52	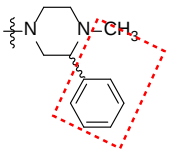	**7.15** ± 2.35[f]	293 ± 55[f]	>1000 (15%)[g]	>1000 (-2%)[g]	40
94 PSB-601[56]	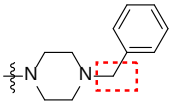	**3.6**	484	2067	>1000	130
95[37]	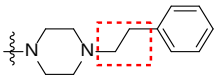	**7.51**	271	>10000	>1000	40

[a] vs. [^{3}H]PSB-603 (n = 3); [b] vs. [^{3}H]MSX-2 (n = 3); [c] vs. [^{3}H]CCPA (n = 3); [d] vs. [^{3}H]PSB-11 (n = 3); [e] selectivity index was calculated by dividing the second lowest K_i value by the A_{2B}AR K_i value; [f] extrapolated curve; [g] percent inhibition of radioligand binding at 1 μM.

Substitution of the aromatic ring

A large variety of substitutions on the aromatic ring were then explored for both benzyl- and phenyl- piperazine derivatives, ranging from lipophilic to polar residues.

Mono-substitution on the aromatic ring

A lipophilic substituent on the *o*-, *m*-, or *p*-position of the phenyl ring, such as F (**29**, **30**, **31**, **96**, **97**), Cl (**9**, **32**, **33**, **98**, **99**), Br (**16**, **17**, **34**, **35**, **36**), I (**37**), Me (**19**, **39**, **40**, **101**), OMe (**18**, **38**, **100**, **104**), N_3 (**20**) or CF_3 (**102**, **103**) was tolerated in benzyl- and phenyl-substituted piperazine derivatives (see Table 5 and Fig. 5A). On the other hand, hydrophilic functional groups (COOH or

OH) at the *p*-position, as in compounds **21** and **41**, led to dramatically decreased potency at the A_{2B}AR, also resulting in lower selectivity. In Fig. 5, it is clearly demonstrated that lipophilic substituents are preferred for high A_{2B}AR affinity as compared to more polar ones, which is likely attributed to the existence of a lipophilic binding pocket in the A_{2B}AR, in which the phenyl ring is accomodated, with bromine leading to the highest potency. It can also be observed, that the more rigid phenylpiperazines in combination with *p*-substituents that are bulker than F, e.g. Br, Cl, Me, OMe, were significantly more selective than the correspoinding benzylpiperazine derivatives (Fig. 5B).

Compounds **20**, **21**, and **41** containing N_3, COOH and OH residues respectively, were designed as functionalized congeners that could be coupled to fluorescent dyes, small peptides, proteins, nucleotides, or other moieties for labeling. Even though the potency was moderate for the polar compounds **21** (COOH) and **41** (OH), the functionalized products will be less polar, and these functionalized compounds are therefore still expected to be very promising for further derivatization. Compounds **22**, **23**, and **51**, which are bearing a longer terminal chain, were found to be better tolerated by the A_{2B}AR than **41** with a free phenolic group, confirming that functionalization on the tail was feasible.

Substitution at the *m*- or *p*-position of either benzyl- or phenyl-piperazine derivatives was favorable in comparison with substitution at the *o*-position. Interestingly, we found that the rank order of potency for *p*-halogen-substituted phenylpiperazine derivatives was as follows: Br (**34**, 0.0835 nM) ≥ I (**37**, 0.159 nM) ≥ Cl (**9**, 0.553 nM) ≥ F (**29**, 0.644 nM). A similar rank order was noticed for benzylpiperazine derivatives: Br (**16**, 0.153 nM) > Cl (**98**, 0.393 nM, p = 0.0081 **) ≥ F (**96**, 0.595 nM). This phenomenon indicates the existence of a halogen bonding interaction. In fact, according to homology modeling and docking studies, a halogen bond with a carbonyl function of a backbone

amino acid residue in transmembrane domain1 (TM1, near the *N*-terminal region), is likely, which will be discussed in detail below. Bromophenyl derivative **34** exhibited an outstanding potency with a K_i value of 0.0835 nM (pK_i = 10.08) and over 10000-fold selectivity versus all other AR subtypes. The affinity of this compound is almost one order of magnitude higher than that of the lead structure PSB-603 (p = 0.0017 **) and may be the most potent A_{2B}AR antagonist known to date.

Table 5. Adenosine receptor affinities of xanthine-8-yl-benzenesulfonamide derivatives with mono-substitution of the phenyl/benzyl ring.

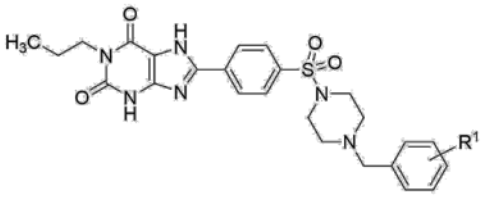

16-23, 77, 94, 96-103

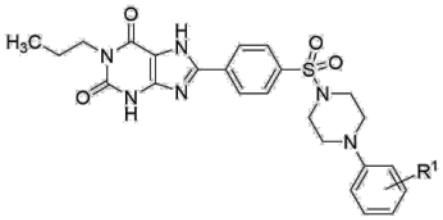

9, 28-41, 51, 104

Compd.	**R^1**	***K*i ± SEM (nM)** (or % inhibition of radioligand binding at indicated concentration)				**Selectivity Index**[e]
		human A_{2B}[a]	**human A_{2A}**[b]	**human A_1**[c]	**human A_3**[d]	
Substitutions on the benzyl ring						
94[56]	H	**3.6**	484	2067	>1000	130
96[37]	4-F	**0.595**	244 ± 3[f, g]	9090 ± 1260[f, g]	758	410
97[37]	3-F	**0.446**	278	2300	>1000	620
98 (PSB-0788)[37]	4-Cl	**0.393**	333	2240	>1000	850
99[37]	3-Cl	**0.782**	161	1090	24200	210
16	4-Br	**0.153** ± 0.004	77.8 ± 11.7[f]	>1000 (31%)[h]	>1000 (28%)[h]	510
17	3-Br	**0.148** ± 0.039	92.4 ± 12.0	928 ± 231[f]	>1000 (23%)[h]	620
100[37]	4-OMe	**0.944**	328	>10000	>10000	350
18	3-OMe	**1.28** ± 0.21[f]	131 ± 15[f]	205 ± 13[f]	>1000 (27%)[h]	100

101[37]	4-Me	**0.858**	212 ± 10[f, g]	398 ± 152[f, g]	156	180
19	3-Me	**0.397** ± 0.119	189 ± 31	795 ± 201[f]	>1000 (17%)[h]	480
102 [37]	4-CF_3	**0.303**	145	5630	>10000	480
103 [37]	3-CF_3	**0.775**	306	2610	30000	400
20	4-N_3	**0.244** ± 0.122	208 ± 51	492 ± 89[f]	>1000 (32%)[h]	850
21	4-COOH	**96.7** ± 14.4	1160 ± 160	>1000 (12%)[h]	>1000 (-7%)[h]	10
22	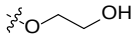	**12.2** ± 4.0	241 ± 49	560 ± 13[f]	>1000 (17%)[h]	20
23	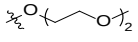	**7.02** ± 1.1	314 ± 74	1010 ± 250	>1000 (30%)[h]	50
Substitutions on the phenyl ring						
28	H	**0.643** ± 0.035	122 ± 32[f]	364 ± 57[h]	>1000 (27%)[h]	190
29	4-F	**0.644** ± 0.154	108 ± 25	>1000 (14%)[h]	>1000 (38%)[h]	170
30	3-F	**0.632** ± 0.178	>1000 (38%)[h]	>1000 (34%)[h]	>1000 (44%)[h]	>1580
31	2-F	**3.22** ± 1.39	>1000 (27%)[h]	>1000 (13%)[h]	>1000 (9%)[h]	>310
9 (PSB-603) [37]	4-Cl	**0.553**	>10000	>10000	>10000	>18080
32	3-Cl	**0.342** ± 0.077	1000 (42%)[h]	>1000 (21%)[h]	53.5 ± 13.7	160
33	2-Cl	**0.403** ± 0.089	204 ± 62	>1000(25%)[h]	>1000(32%)[h]	510
34 (PSB-1901)	4-Br	**0.0835** ± 0.0327	>1000 (33%)[h]	>1000 (13%)[h]	>1000 (29%)[h]	>11980
35	3-Br	**0.234** ± 0.069[f]	>1000 (24%)[h]	>1000 (-1%)[h]	>1000 (27%)[h]	>4270
36	2-Br	**0.137** ± 0.033	89.5 ± 5.4	>1000 (28%)[h]	>1000 (20%)[h]	650
37	4-I	**0.159** ± 0.066	2990 ± 1133[f]	>1000 (24%)[h]	>1000 (36%)[h]	>6290
104[37]	4-OMe	**1.99**	3720	>10000	>1000	>500
38	3-OMe	**0.616** ± 0.092	197 ± 45[f]	>1000 (-3%)[h]	>1000 (-1%)[h]	320
39	4-CH_3	**0.706** ± 0.141	>1000 (34%)[h]	>1000 (12%)[h]	>1000 (25%)[h]	>1420
40	2-CH_3	**0.432** ± 0.116	140 ± 26	419 ± 62[f]	>1000 (25%)[h]	320
41	4-OH	**4.30** ± 0.81	96.7 ± 3.9	356 ± 92[f]	>1000 (21%)[h]	20
51	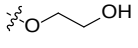	**6.08 ±** 1.23	168 ± 5	>1000 (24%)[h]	>1000 (23%)[h]	30

[a] vs. [^{3}H]PSB-603 (n = 3); [b] vs. [^{3}H]MSX-2 (n = 3); [c] vs. [^{3}H]CCPA (n = 3); [d] vs. [^{3}H]PSB-11 (n = 3); [e] the selectivity index was calculated by dividing the second lowest K_i value by the A_{2B}AR K_i

value; [f] extrapolated curve; [g] data obtained in this study; [h] percent inhibition of radioligand binding at 1 μM.

A.

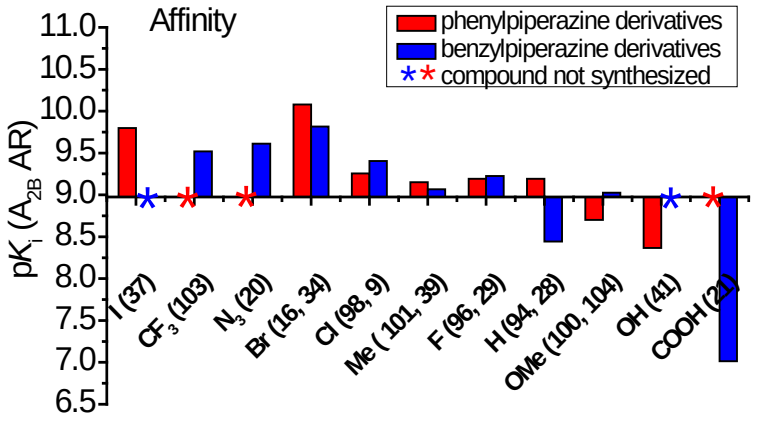

B.

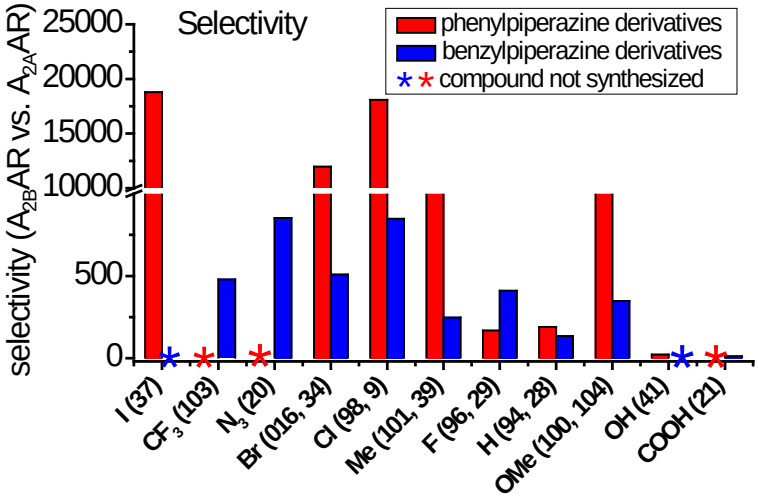

Figure 5. Effects of substituents in the *p*-position of phenylpiperazine (red bars) and benzylpiperazine (blue bars) derivatives. **A.** Affinities of compounds at human A_{2B}ARs determined in radioligand binding assays are given as pK_i values. **B.** A_{2B}AR selectivity versus the A_{2A}AR.

Di-substitution on the aromatic ring

Next, we investigated combination of two substituents on the aromatic ring in benzyl- and phenylpiperazines (Table 6). Di-substitution with small residues was found to be very well tolerated in different positions, e.g. F and OMe in compounds **24**-**26** and **45**, Cl and OMe in compounds **46** and **47**, F and Cl or Br in compounds **50** and **27**. However, combinations were not synergistic, and the combination of two favourable substituents did not appear to increase affinity over that of mono-substituted analog (compare, for example, **16**/**77**). However, some 3,4-di-substitutions resulted in increased A_{2A}, and in some cases also A_1 affinities, and reduced A_{2B} selectivity, e.g. **105** (3,4-methylenedioxy; K_i A_{2B} 1.06 nM, K_i A_{2A}AR 112 nM), **48** (3-Cl, 4-OH; K_i A_{2B} 3.55 nM, A_{2A} 93.8 nM) and **49** (4-Cl, 3-OH; K_i A_{2B} 0.215 nM, A_{2A} 35.3 nM, A_1 113 nM). Potency comparisons between di-substituted compounds and each of the respective mono-substitued compounds are depicted in Fig. 6. In most cases, affinities of the di-substituted derivatives with small substituents were similar to those of the mono-substituted analogs, while the selectivity indices were interdependently differing.

Table 6. Adenosine receptors affinities of xanthine-8-yl-benzenesulfonamide derivatives with di-substitution of the phenyl/benzyl ring.

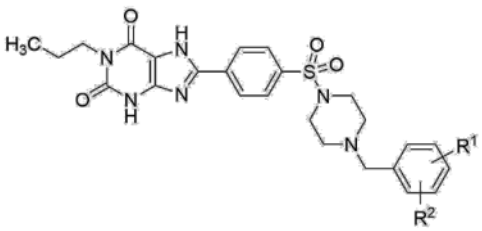

24-27, 105

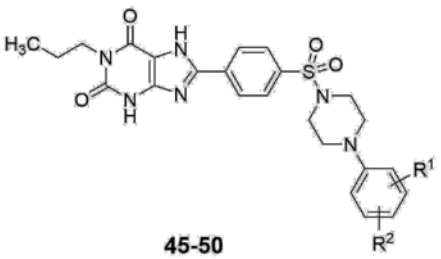

45-50

Compd.	R^1	R^2	K_i ± SEM (nM) (or % inhibition of radioligand binding at indicated concentration)				Selectivity Index[e]
			human A_{2B}[a]	human A_{2A}[b]	human A_1[c]	human A_3[d]	

Substitutions on the benzyl ring							
26	3-F	5-OMe	**1.02** ± 0.35	160 ± 45	>1000 (31%) [f]	>1000 (12%)[f]	160
24	3-F	4-OMe	**0.894** ± 0.173[g]	245 ± 35	>1000 (24%) [f]	>1000 (15%)[f]	270
25	4-F	3-OMe	**0.629** ± 0.031	135 ± 36	>1000 (25%) [f]	>1000 (-5%)[f]	220
27	3-F	4-Br	**0.473** ± 0.076	403 ± 6	326 ± 49[g]	>1000 (27%)[f]	690
105 [37]	3,4-methylenedioxy		**1.06**	112	443	17600	110
Substitutions on the phenyl ring							
45	3-F	4-OMe	**1.24** ± 0.03	>1000 (30%)[f]	>1000 (34%) [f]	>1000 (21%)[f]	>800
46	3-Cl	4-OMe	**0.352** ± 0.072	>1000 (31%)[f]	>1000 (23%) [f]	>1000 (1%) [f]	>2840
47	4-Cl	3-OMe	**0.215** ± 0.067	35.3 ± 8.2	535 ± 250	>1000 (46%)[f]	160
48	3-Cl	4-OH	**3.55** ± 0.77	93.8 ± 17.7 [g]	>1000 (37%) [f]	>1000 (41%)[f]	>30
49	4-Cl	3-OH	**0.421**± 0.041	40.7 ± 10.4	113 ± 39	>1000 (31%)[f]	100
50	2-F	4-Cl	**1.91** ± 0.47	>1000 (6%)[f]	>1000 (9%)[f]	>1000 (14%)[f]	>500

[a] vs. [^{3}H]PSB-603 (n = 3); [b] vs. [^{3}H]MSX-2 (n = 3); [c] vs. [^{3}H]CCPA (n = 3); [d] vs. [^{3}H]PSB-11 (n = 3); [e] the selectivity index was calculated by dividing the second lowest K_i value by the A_{2B}AR K_i value; [f] percent inhibition of radioligand binding at 1 μM; [g] extrapolated curve.

A.

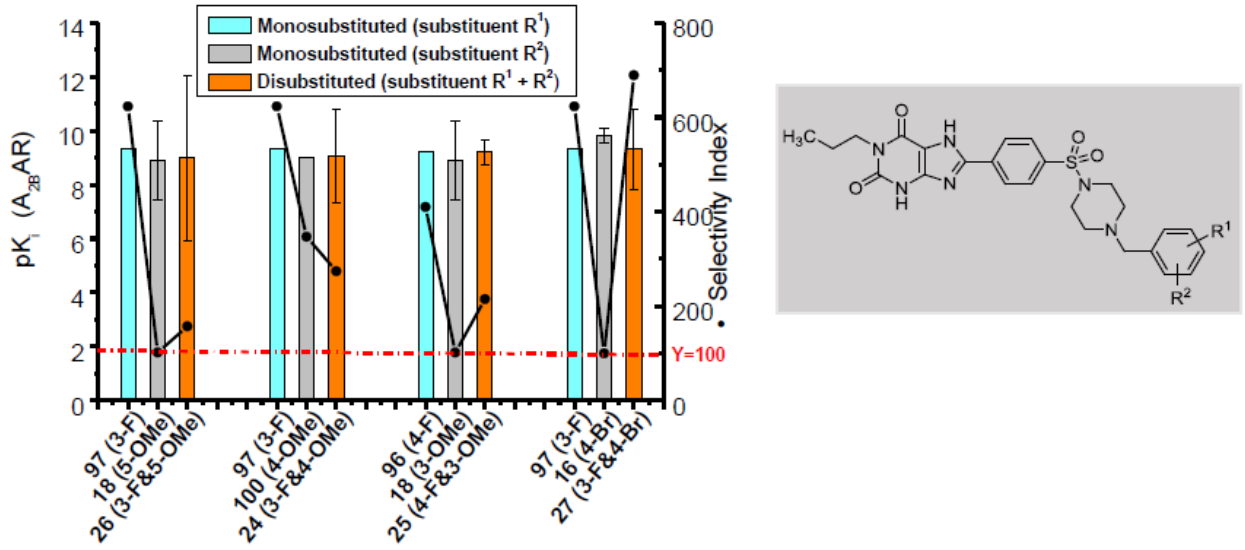

B.

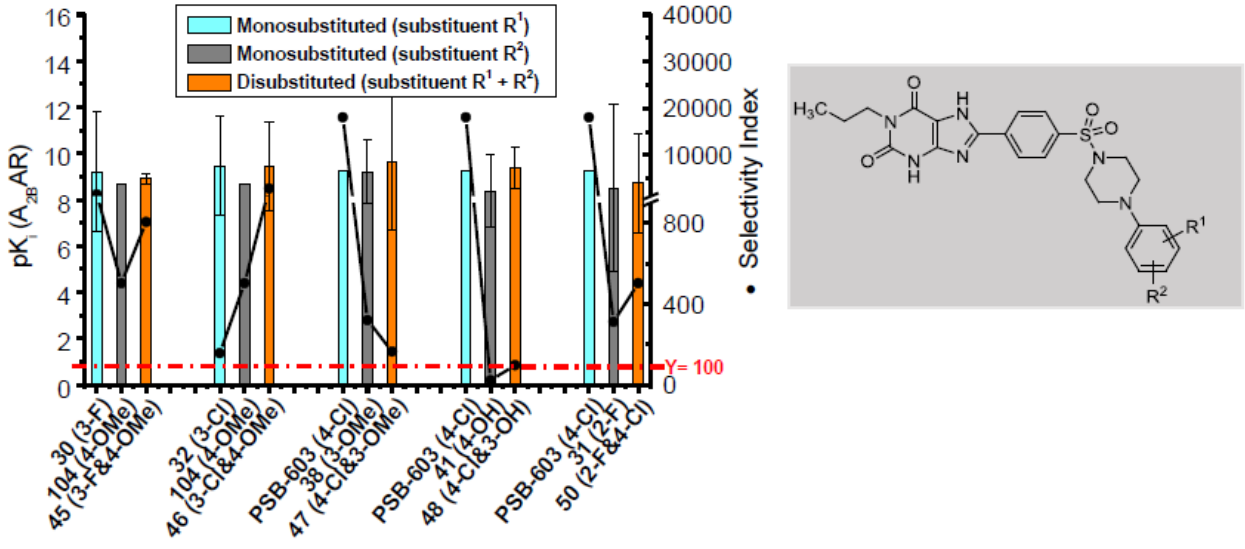

Figure 6. Potency comparisons between mono-substituted and di-substituted derivatives of **A**. benzyl-piperazines, and **B**. phenyl-piperazines. The left Y-axis represents the pK_i value at the A_{2B}AR for benzyl and phenyl derivatives (blue and gray bar: mono-substituted compounds, orange bar: di-substituted compounds); the right Y-axis represents the selectivity index.

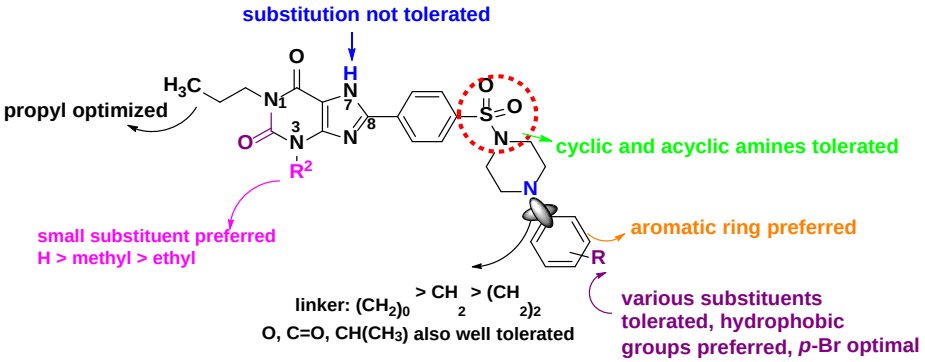

Figure 7. Structure-activity relationships of xanthine-8-yl-benzenesulfonamide derivatives as antagonists of the A_{2B}AR.

Figure 7 summarizes the structure-activity relationships of the investigated compounds as antagonists of the A_{2B}AR: (i) small substituents, like methyl and ethyl, are well tolerated at *N*3 of the xanthine core even though a free NH is preferred, not only with regard to affinity, but also for selectivity; (ii) various secondary and tertiary amines for sulfonamide formation are tolerated, and substituted phenylpiperizine derivatives show the highest potency; (iii) various substitutions or modifications of the linker between the piperazine moiety and the aromatic ring are also well tolerated, no linker as in phenylpiperazine derivatives leading to the most potent and selective derivatives; (iv) various substituents including combinations with hydrophobic groups on the terminal phenyl ring are well tolerated, with *p*-substituted derivatives resulting in the highest potency.

Investigation of Potential Species Differences

Preclinical experiments, including target validation studies, are mostly performed in rodents, very often in mice. Previous studies have shown that many AR ligands display significant species differences in potency and selectivity. [13, 32, 62] To investigate potential species differences of selected compounds, we determined their affinity for all mouse AR subtypes in addition to the

human ARs (see Table 7 and Fig. 8). Compounds **14**, **17**, and **30** showed high affinity and selectivity (>100-fold versus other ARs) at both human and mouse receptors with only 1.5- to 6-fold lower A_{2B}AR affinity for the mouse as compared to the human receptor. The most potent A_{2B}AR antagonist, **34** was potent and selective for the human as well as the mouse A_{2B}ARs with outstanding K_i values for the A_{2B}ARs in both species (K_i 83.5 pM (human), 131 pM (mouse), >7000- fold selectivity). Since the current standard A_{2B}AR antagonist **9** was found to display some affinity for the mouse A_1ARs (42.4 nM), but being still 160-fold selective for the A_{2B} over the A_1AR in mice,[32] compound **34** appears to be even superior for A_{2B}AR studies in mice. Concentration-inhibition binding curves at human and mouse A_{2B}ARs are depicted in Figure 8.

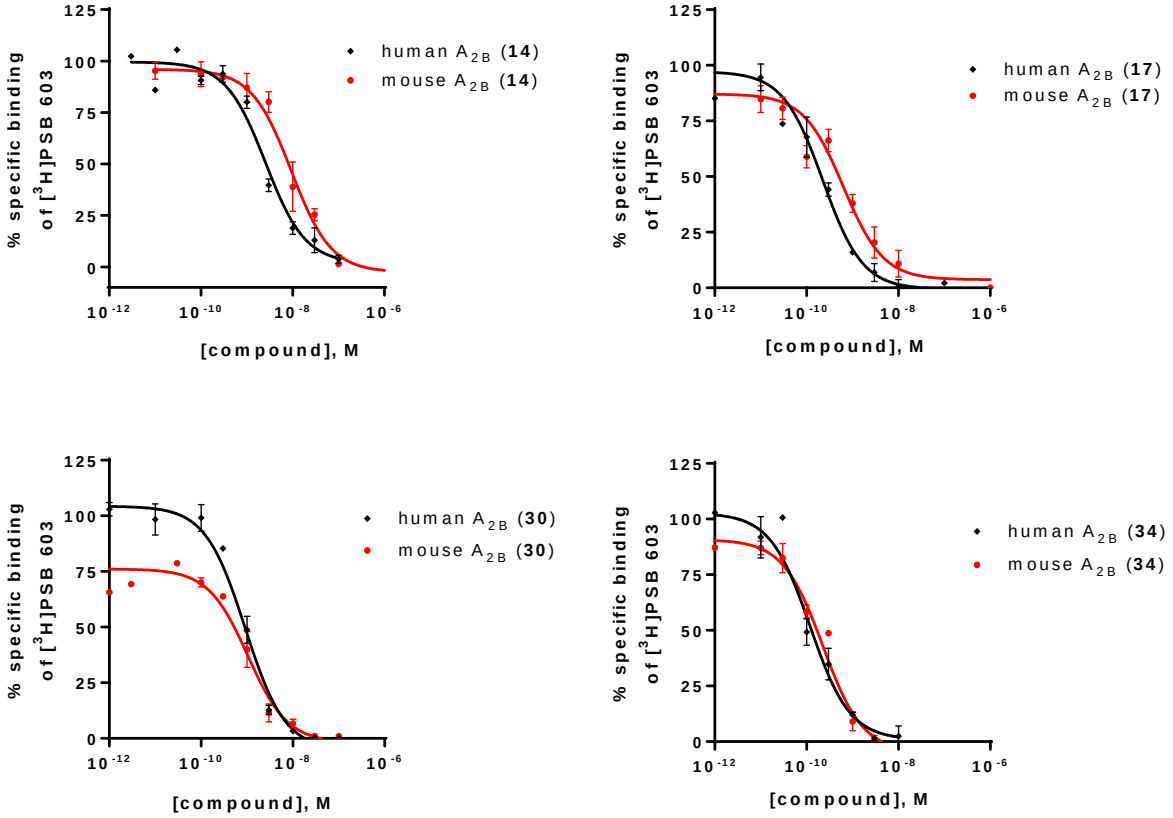

Figure 8. Competition binding experiments. Concentration-dependent inhibition of 0.3 nM [^{3}H]PSB-603 by compounds **14**, **17**, **30**, and **34** at membrane preparations of CHO cells recombinantly expressing human or mouse A_{2B}ARs. Data represent means ± SEM of 3 independent experiments.

Table 7. Comparison of affinities of selected compounds at human and mouse AR subtypes.

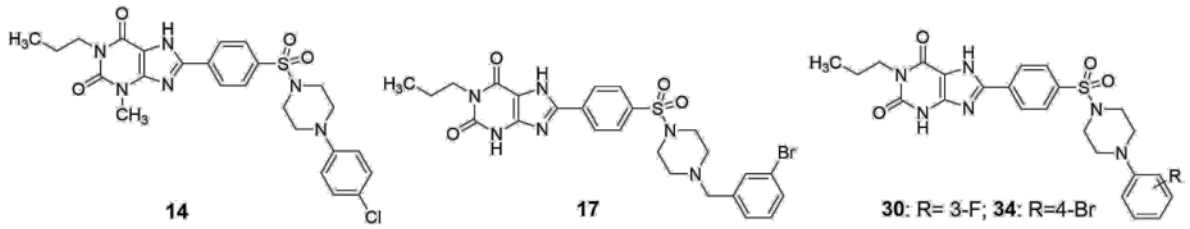

Compd.	Species	K_i ± SEM (nM) (or % inhibition of radioligand binding at 1 μM)				Selectivity Index[f]
		A_{2B}[a]	A_{2A}[b]	A_1[c]	A_3[d,e]	
9[32, 37]	human	**0.553**	>10000	>10000	>10000	>18000
	mouse	**0.265**	>10000	42.4	>10000	160
14	human	**1.91** ± 0.32	>1000 (33%)[g]	>1000 (22%)[g]	>1000 (39%)[g]	>520
	mouse	**8.34** ± 1.14	>1000 (17%)[g]	1520 ± 330	>1000 (-1%)[g]	>180
17	human	**0.148** ± 0.039	92.4 ± 23.0	928 ± 231[h]	>1000 (23%)[g]	620
	mouse	**0.901** ± 0.171	507 ± 84	107 ± 6	>1000 (5%)[g]	120
30	human	**0.632** ± 0.178	>1000 (38%)[g]	>1000 (34%)[g]	>1000 (44%)[g]	>1580
	mouse	**0.926** ± 0.202	>1000 (40%)[g]	>300 (46%)[g]	>1000 (-2%)[g]	>320
34	human	**0.0835** ± 0.0327	>1000 (33%)[g]	>1000 (13%)[g]	>1000 (29%)[g]	>11970
	mouse	**0.131** ± 0.047	>1000 (6%)[g]	>1000 (29%)[g]	>1000 (8%)[g]	>7630

[a] vs. [^{3}H]PSB-603 (n = 3) for both human and mouse receptors; [b] vs. [^{3}H]MSX-2 (n = 3) for both human and mouse receptors; [c] vs. [^{3}H]CCPA (n = 3) for both human and mouse receptors; [d] vs. [^{3}H]PSB-11 (n = 3) for the human receptor;[e] vs. [^{3}H]NECA (n = 3) for the mouse receptor; [f] selectivity index was calculated by dividing the second lowest K_i value by the A_{2B}AR K_i value; [g] percent inhibition of radioligand binding at 1 μM; [h] extrapolated curve.

cAMP accumulation assays

In order to evaluate the functional properties of the antagonists, the ability of selected compounds (**14**, **17**, **30**, and **34**) to inhibit NECA-stimulated cAMP production was measured in CHO cells stably transfected with the human A_{2B}AR.

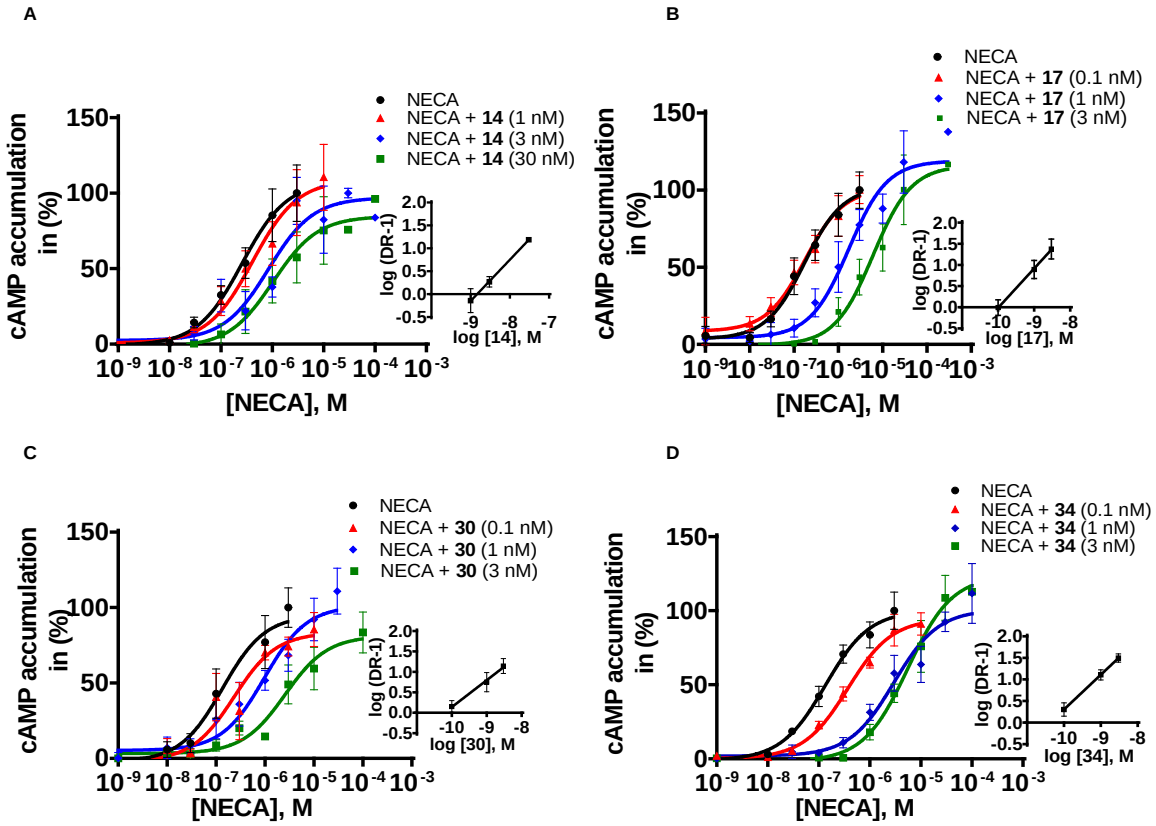

Figure 9. cAMP accumulation experiments at CHO cells stably expressing the human A_{2B}AR. Cells were stimulated with the agonist NECA in the absence or presence of different concentrations of antagonist (**14**, **17**, **30**, or **34**, respectively). NECA displayed an EC_{50} value of ca. 200 nM. Data were normalized to the maximal effect induced by NECA (observed at 3 μM NECA in the absence of antagonist), set at 100 %. Data represent means ± SEM of 3-4 independent experiments. The

calculated K_B-value from the Schild equation was 1.61 ± 0.16 nM for 14, 0.201 ± 0.022 nM for **17**, 0.167 ± 0.018 nM for 30, and 0.0598 ± 0.0153 nM or **34**. Schild plots are shown as insets.

In the presence of different concentrations of the investigated antagonists, NECA curves were significantly shifted to the right whereas the efficacy of NECA remained unaltered indicating competitive antagonism as shown in Figure 9. The K_B-values for the different antagonists calculated by the Schild equation revealed an excellent correlation with the K_i-values determined in radioligand binding experiments as shown in Figure 10.

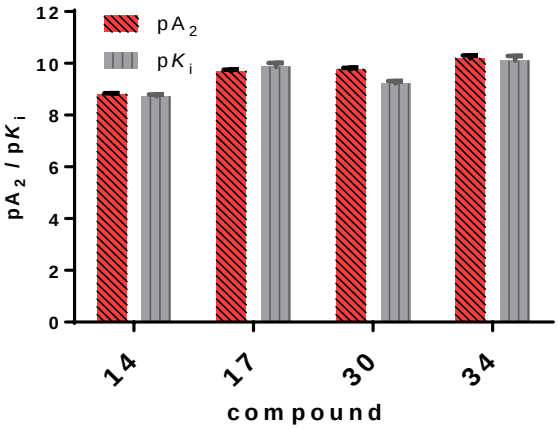

Figure 10. pA_2 values for antagonists **14**, **17**, **30**, and **34** determined in cAMP accumulation assays in CHO cells stably expressing the human A_{2B}AR compared to pK_i values determined in radioligand binding assays at human A_{2B}ARs (n = 3-4). Error bars correspond to SEM values.

Homology modeling and docking studies

To better understand the molecular interactions of the synthesized compounds, and in particular, the effect of substituents on the terminal aromatic ring, an updated homology model of the human

A_{2B}AR was developed. It was based on the crystal structure of the human A_{2A}AR at high resolution (1.8 Å) in complex with the antagonist ZM241385 (PDB ID: 4EIY).[63]

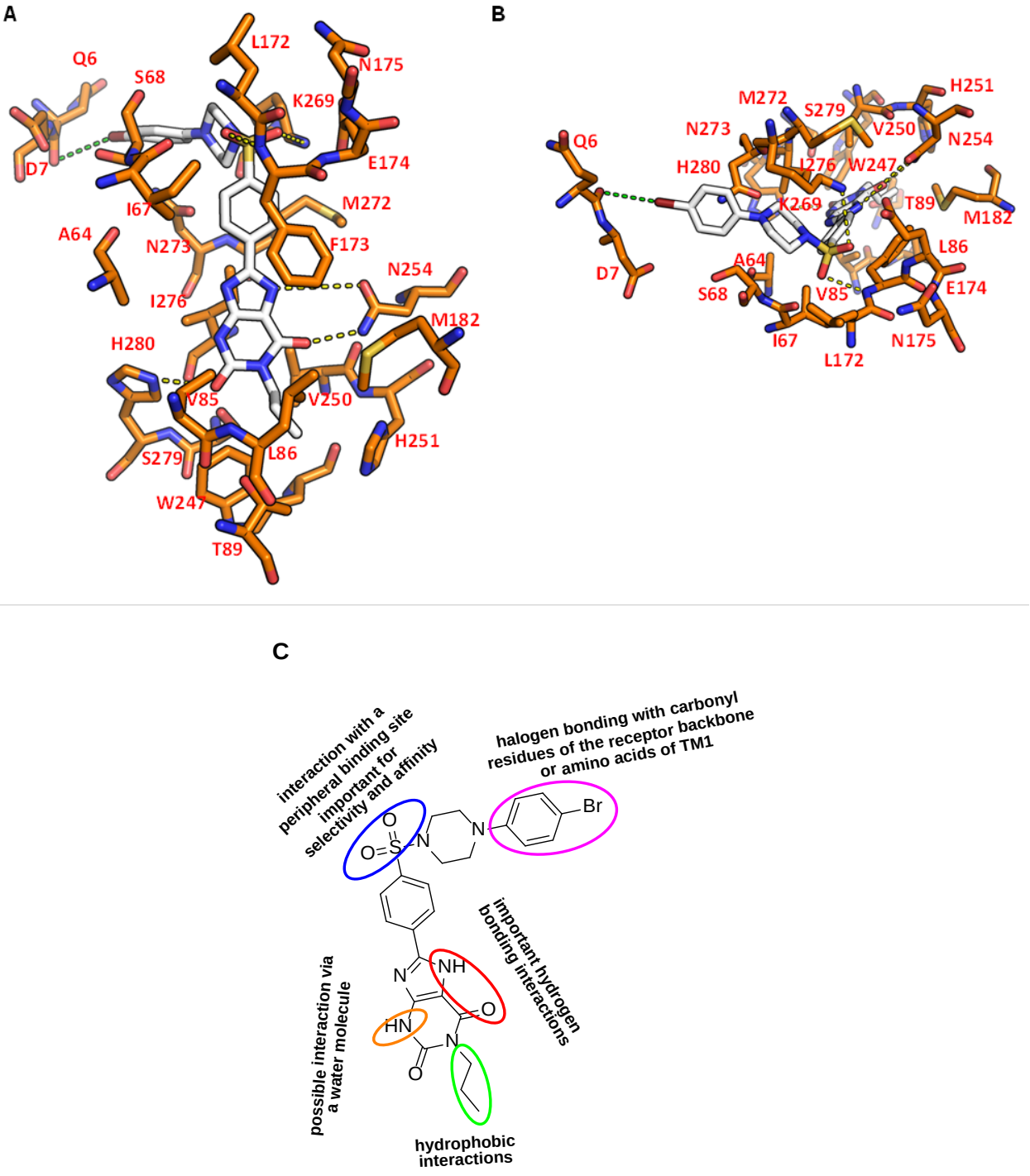

Figure 11. Proposed binding mode of compound **34** (PSB-1901, silver) in a homology model of the human A_{2B}AR (based on the X-ray structure of the human A_{2A}AR, PDB ID 4EIY) with the important residues shown (orange) in the putative binding pocket. **A**. Side view of **34** in the binding pocket with the extracellular receptor domains on the top. **B**. Top view of **34** in the binding pocket. Oxygen atoms are colored in red, nitrogen atoms in blue, sulfur atoms in yellow, and bromine in maroon. The proposed hydrogen bond interactions are depicted as yellow dotted lines, and the halogen bond is indicated in green dotted lines. **C**. Proposed interactions of xanthine derivative **34** which exhibits the highest binding affinity for the human A_{2B}AR of the present series of compounds, combined with high subtype-selectivity.

The putative binding mode of potent antagonist **34** and selected residues in the binding pocket of the human A_{2B}AR that may be important for interaction are shown in Figure 11. Apparently, the xanthine core is anchored within the binding cleft through hydrogen bond interaction with Asn254. In addition, the *C*6-carbonyl and the *N*7-H of the xanthine core interact with the side chain of Asn254. The proposed hydrogen bond interaction motif with Asn254 is conserved among all human AR subtypes (see Supporting Information, Figure S19.) The xanthine core was found to occupy a pocket formed by Ala64, Ile67, Val85, Leu86, Phe173, Met182, Trp247, Val250, His251, Asn254, Ile276, Ser279, and His280. Among these residues, Val250 is unique for the human A_{2B}AR (Leu in other AR subtypes) and may improve the affinity towards the human A_{2B}AR in comparison to other subtypes of ARs. The propyl group at position 1 of the xanthine core is directed towards a hydrophobic subpocket formed by Val85, Leu86, Thr89, Met182, Trp247 and Val250 in the receptor model. Among these residues forming hydrophobic interactions, the highly conserved Trp247 is a residue that is important for AR activation and antagonist binding.[64] The *C*2-carbonyl

group forms a hydrogen bond interaction with His280. The free N3-H of the xanthine core did not show any direct interaction to the amino acid residues in the binding pocket in our model. A closer visual inspection of the binding mode of **34** revealed a potential position for a water molecule in the region between the free N3-H of **34** and the residues Ala64, Val85, Ile276, and His280. This position corresponds to a water molecule observed in the crystal structure of the human A_{2A}AR in complex with the antagonist ZM241385 (see Supplementary Figure S20). [63] Possibly, the water molecule is positioned in the binding pocket and forms an interaction with the free *N*3-H thereby improving the potency of **34**. This is in agreement with the SARs showing that substitution of *N*3 decreases binding affinity. Similar interactions were predicted for the 3,4-dihydropyrimidin-2(1*H*)-one scaffold previously developed as antagonists for the human A_{2B}AR.[30] The obtained binding mode of **34** also indicated that the aromatic ring system of the benzenesulfonamide residue or that of the xanthine core is probably stabilized through a π-π interaction with Phe173. An electrostatic interaction between the sulfonyl group and the basic amino acid residue Lys269 is feasible. Lys269 is one of the unique amino acid residues in the human A_{2B}AR, and its interaction with the antagonist possibly increases binding affinity and selectivity. In our model, the sulfonyl group also forms an interaction with the main chain of Phe173. The side-chain of Glu174 located at a distance of ~3.5 Å might be involved in the interaction with the sulfonyl group and thereby contribute to its binding affinity. The *p*-bromophenylpiperazine residue of **34** is predicted to be directed towards the solvent-exposed extracellular region and positioned in close proximity to the amino acid residues Gln6, Asp7, Ser68, Leu172, Lys269, Met272 and Asn273. Ser68 is conserved in both, the human A_{2B}AR and the human A_{2A}AR, and the serine residue probably attracts one of the nitrogen atom of the piperazine ring in the piperazine-substituted xanthine derivatives and introduces an additional interaction. Such an interaction possibly decreases the effect of interactions between the sulfonyl group and Lys269. While the serine interaction with the piperazine *N*- atom might decrease the

compounds' selectivity, the high affinity and subtype-selectivity of **34** for the human A_{2B}AR might be explained by the formation of a halogen bond with a carbonyl residue of the backbone of the receptor or amino acids of TM1 (near the *N*-terminal region). Halogen bonds are medium to strong interactions that can compete or act synergistically with weak to moderately strong hydrogen bonds.[65] Furthermore, halogen bonding is driven by the anisotropy of electron density (which induces a partial positive charge, σ-hole) on the halogen atom (chlorine, bromine, iodine). For fluorine atoms, a positive potential can only be observed in special cases because of the high electronegativity. With respect to a chlorine or bromine substituent, formation of a halogen bond occurs, if the distance is about 3.27 Å (Cl···O) or 3.37 Å (Br···O) and the angle is close to 180°.[65, 66] In the constructed homology model (human A_{2B}AR-**34** complex) a comparable distance 4.08 Å and an angle of 163.1° was observed between the backbone carbonyl group of Gln6 and the bromine substituent. For the chlorine substituent the distance was calculated to be about 4.27 Å and the same angle of 163.7° was observed. The difference of the calculated distance in the docked complex is comparatively lower for Br (0.71 Å) than for Cl (1.0 Å) and the bromine-substituted derivative **34** possibly forms a much strong halogen bond interaction as compared to the chloro-substituted derivative **9**, which is expected to form only a weak or no interaction. The strong halogen bond could possibly reduce the attraction of the piperazine moiety of **34** towards the serine residue (Ser68). This halogen-bonding hypothesis is underpinned by the improved binding affinity (K_i = 0.0835 nM) of compound **34** substituted with Br (Figure 11A and 11B) in comparison to compounds substituted with F (**29**), Cl (**9**, PSB-603) or CH_3 (**39**) with binding affinities (K_i values) following the rank order: Br (**34**, 0.0835 nM) > Cl (**9**, 0.553 nM, p = 0.0122*) ≥ F (**29**, 0.644 nM) ≥ CH_3 (**39**, 0.706 nM). A small decrease in binding affinity was observed for the iodine-substituted derivative **37** (K_i = 0.159 nM), which implies that the distance between the halogen atom and the backbone carbonyl group of the receptor is not optimal. Based on the docking analysis and

experimental results, the characteristics of **34** as a high-affinity antagonists at the human A_{2B}AR with very high subtype-selectivity are shown in Figure 11C.

CONCLUSIONS

In this study, we thoroughly explored the SARs of xanthin-8-yl-benzenesulfonamides mainly by exploring different linkers for attaching a terminal phenyl ring and by introducing a variety of substituents. A new synthetic strategy was established by reaction of sulfonamide-substituted benzoic acid derivatives, prepared from piperazine derivatives and 4-(chlorosulfonyl)benzoic acid, with substituted 5,6-diaminouracils followed by ring closure to the corresponding xanthines in the presence of P_2O_5 for 10 min as a condensing agent. This new convergent method was found to be superior to the previously developed linear synthetic procedure.

Many of the new A_{2B}AR antagonists exhibited subnanomolar affinity and high selectivity versus the other AR subtypes. Disubstitution of the sulfonamide *N*-atom contributed to increased selectivity for the A_{2B}AR and piperazine derivatives were preferred. A shorter linker between the piperazine ring and the terminal aromatic ring led to increased potency. Lipophilic substituents on the aromatic ring resulted in increased potency. The *p*-bromophenylpiperazine-substituted derivative **34** represents the most potent and selective A_{2B}AR antagonist described to date, with K_i values of 0.0835 nM for the human A_{2B}AR, determined in radioligand binding assays, and >10,000-fold selectivity. It was similarly potent and selective for the mouse A_{2B}AR, making it a promising pharmacological tool for preclinical studies, being superior to the current standard A_{2B}AR PSB-603 (**9**), not only with regard to A_{2B} affinity, but especially because of its exceptional selectivity in mouse. In cAMP assays at the human A_{2B}AR, **34** displayed a K_B value of 0.0598 nM which

correlates well with its binding data. Computational studies predicted halogen bonding to contribute to the outstanding potency of **34**. Interactions with amino acid residues near the extracellular region, distant from the orthosteric binding site, were proposed as a reason for the extraordinarily high selectivity of **34** and many of its analogs.

Moreover, we successfully introduced functional groups attached to the terminal phenyl ring, e.g. azido, carboxy and hydroxy functions, some attached via a (di)ethyleneglycol linker, which were tolerated by the A_{2B}AR, and can be used for future labeling with fluorescent dyes or other reporter groups.

The developed antagonists will be useful tools for in vitro and in vivo studies and provide new insights into the SARs and binding interactions of A_{2B}AR antagonists, which hold great promise as future drugs, especially in immuno-oncology, chronic inflammatory and infectious diseases.

EXPERIMENTAL SECTION

1. Chemistry

General. All commercially available reagents were obtained from various producers (Acros, Aldrich, Fluka, Merck, and Sigma) and used without further purification. Solvents were used without additional purification or drying. Reactions were monitored by thin-layer chromatography (TLC) using aluminum sheets coated with silica gel 60 F_{254} (Merck). Column chromatography was performed with silica gel 0.060-0.200 mm, pore diameter ca. 6 nm. Preparative HPLC was carried out on a Knauer HPLC system with a Wellchrome K-1800 pump, a WellChrome K-2600 spectrophotometer, and a Eurospher 100 C18 column (250 mm × 20 mm, particle size 10 μm). A gradient of methanol in water was used as indicated below with a flow rate of 15 mL/min. Lyophilisation was performed with a CHRIST ALPHA 1-4 LSC freeze dryer.

The purity of all measured compounds was determined by HPLC-UV obtained on an LC-MS instrument (Applied Biosystems API 2000 LC-MS/MS, HPLC Agilent 1100) using the following procedure: Compounds were dissolved at a concentration of 0.5 mg/mL in methanol/H_2O/NH_3(aq) (1:1:0.1). Then, 10 μL of the sample were injected into a Phenomenex Luna C18 HPLC column (50 mm × 2.00 mm, particle size 3 μm) and chromatographed using a gradient of water/methanol (containing 2 mM ammonium acetate) from 90:10 to 0:100 for 20 min at a flow rate of 250 μL/min. UV absorption was detected from 200 to 950 nm using a diode array detector. Mass spectra were recorded on an API 2000 mass spectrometer (electron spray ion source, Applied Biosystems, Darmstadt, Germany) coupled with an Agilent 1100 HPLC system. For all other intermediate compounds, the same method was used, but the compounds were dissolved in methanol.

High-resolution mass spectra (HRMS) were recorded on a micrOTOF-Q mass spectrometer (Bruker) with ESI-source coupled with an HPLC Dionex Ultimate 3000 (Thermo Scientific) using an EC50/2 Nucleodur C18 Gravity 3 μm column (Macherey-Nagel). The column temperature was 25 °C. Ca. 1 μL of a 1 mg/mL solution of the sample in acetonitrile was injected and a flow rate of 0.3 mL/min was applied. HPLC was started with a solution of acetonitrile in water (10:90) containing 2 mM CH_3COONH_4. The gradient was started after 1 min reaching 100 % acetonitrile within 9 min and then flushed at this concentration for another 5 min. Purities of all products were determined by HPLC-UV-MS and proven to be ≥ 95 %.

^{1}H- and ^{13}C-NMR data were collected on a Bruker Avance 500 MHz NMR spectrometer at 500 MHz (^{1}H), and 126 MHz (^{13}C), or on a 600 MHz NMR spectrometer at 600 MHz (^{1}H), and 151 MHz (^{13}C). $CDCl_3$ or DMSO-d_6 was used as solvent. Chemical shifts are reported in parts per million (ppm) relative to the deuterated solvent, i.e. DMSO, ^{1}H: 2.49 ppm; ^{13}C: 39.7 ppm; chloroform, δ ^{1}H: 7.26 ppm; ^{13}C: 77.36 ppm. Coupling constants J values are given in Hertz and spin multiplicities are given as s (singlet), d (doublet), t (triplet), m (multiplet), br (broad) or variations thereof.

1.1 Procedures for synthesis of compounds 14-44 and 50-54

The synthesis of the final products can be divided into three steps: 1. synthesis of the *p*-nitrophenylsulfonylphenylxanthine derivative (**13a-c**); 2. synthesis of the substituted amine (if not commercially available); 3. coupling of both.

Compound **10a-c**, **12a-c** and **13a-c** were synthesized according to previously described procedures.[37] Detailed synthetic procedures for compound **11** and some of the required amines (**58**, **60**, **62-64**, **81**, **82**, **85-87**, **89**) are described in Supporting Information; they were obtained in analogy to previously described methods[36] with some modifications.

Aminolysis of *p*-nitrophenylsulfonate ester 13a-c: Method A. *p*-Nitrophenylsulfonate **13a** (0.15 mmol) was dissolved in 5 mL of dry DMF, and the appropriate amine (**60**, or **61**, or **63**, or **81**) was added (0.9 mmol, 6 eq.). The reaction mixture was refluxed for 1 h. Then it was poured into 30 mL of water to precipitate the product. The solid was filtered off and then washed with water (3 × 15 mL). The desired pure product was obtained by column chromatography on silica gel 60 using a mixture of methanol and dichloromethane (1 – 5 % MeOH) as an eluent and subsequent recrystallization from dichloromethane (containing 10 % methanol)/petroleum ether. The product was washed with ethanol (3 × 5 mL) and dried at 70 °C. For yields see Table 1.

Method B. *p*-Nitrophenylsulfonate **13a-c** (0.15 mmol) was dissolved in 4 mL of dry DMSO and the appropriate amine (detailed information for the amines see characterization data for the final products below, 1.5 - 2 eq.) was added. The solution was stirred for 3 h at 150 °C under an argon atmosphere. The mixture was poured into 30 mL of water and a precipitate was formed. The solid was filtered off and washed with water (3 × 10 ml), methanol (3 × 5 mL) and diethyl ether (3 × 5 mL). For yields see Table 1. Samples were dissolved in MeOH : H_2O : triethylamine (1:1:0.1) and

further purified by preparative RP-HPLC using a gradient of water : methanol (80:20) to methanol (100 %).

Method C. Compounds were synthesized according to method A to obtain the protected precursors followed by deprotection, yielding the desired final compounds (**21**, **41**).

Compound 21: Compound **21a** was obtained according to method A by using **13a** (0.15 mmol) and ethyl 4-(piperazin-1-ylmethyl)benzoate (**61**, 0.9 mmol). Lithium hydroxide (5 mmol) was added to the suspension of ethyl ester **21a** (540 mg, 0.9 mmol) in a mixture of methanol and tetrahydrofuran (1 : 1; 10 mL). The reaction was left stirring overnight at rt and then concentrated under reduced pressure. The crude product was precipitated by adding diluted acetic acid dropwise, filtered off under reduced pressure and further washed with water. Column chromatography (CH_2Cl_2 : MeOH = 9 : 1) gave 180 mg of a white solid, yielding 23 % over two steps.

Compound 41: Compound **41a**, containing a MOM-protected hydroxy group, was obtained according to method A by using **13a** (0.15 mmol) and 1-(4-(methoxymethoxy)phenyl)piperazine (**81**, 0.9 mmol). To a suspension of **41a** (20 mg, 0.036 mmol) in a solution of dichloromethane : methanol (1:1; 5 mL) were added 4 M HCl in dioxane (1.0 mL). The resulting mixture was stirred at 60 °C for 1h until the reaction was completed. Subsequently, the mixture was concentrated and the product (**41**) was obtained by precipitation through the addition of water, petroleum ether and NaCl solution (15 ml each). The pale gray solid was filtered off under reduced pressure and dried at 70 °C, yielding 21 % over two steps.

Method D. A mixture of **13a** (50 mg, 0.11 mmol, 1 eq.) in 5 mL of dimethylamine (**91**, in ethanolic solution, 33 % v/v) was stirred at rt for 16 h. Subsequently, the reaction mixture was concentrated under reduced pressure. The residue was purified by flash chromatography (eluent:

dichloromethane : methanol = 9:1) giving product **53** as a beige-colored solid in a yield of 29 %.

1.2 New approach of the preparation of compounds 45-49

A new convergent strategy was established, in which the sulfonamide group was attached to the benzoic acid before coupling to the 5,6-diaminouracil derivative. To this end, 4-(chlorosulfonyl)benzoic acid (**11a**) was reacted with **85-87** to obtein the intermediate sulfonamides **85b**-**87b**. The sulfonamide intermediates were subsequently condensed with uracil derivative **10a** to yield **85c-87c**, followed by fast ring closure reaction with P_2O_5 for 10 min, yielding the final products **45-47** (Scheme 2).

Detailed descriptions of the synthesis of piperazines **85-87** are provided in Scheme 2, which were obtained according to a previously reportet method[67] with minor modifications.

General procedure for the preparation of 45-47. To a flask containing 0.43 mmol of **85c-87c** in 5 mL of DMF, 3.17 mmol (900 mg) of P_2O_5 was added. The reaction was refluxed for 10 min. Then, distilled water was added portion-wise until a white precipitate was formed that was further purified by column chromatography.

General procedure for the preparation of 48 and 49. To a flask containing 0.09 mmol (50 mg) of **46** or **47**, 2 mL of BBr_3 in DCM were added. The reaction was stirred under argon for 24 h. A mixture of ice and aqueous $NaHCO_3$ solution (20 mL) was added and the mixture was subsequently extracted with ethyl acetate. The organic layer was dried over anhydrous Mg_2SO_4, filtered, and evaporated to give a crude product which was further purified using column chromatography yielding **48** (25 %) and **49** (13 %), respectively.

1.3 Preparation and characterization of final products (14-54)

8-(4-((4-(4-Chlorophenyl)piperazin-1-yl)sulfonyl)phenyl)-3-methyl-1-propyl-3,7-dihydropurine-2,6-dione (14) Method B. The compound was synthesized using **13b** (0.15 mmol) and 1-(4-chlorophenyl)piperazine (**55**, 0.225 mmol) in 4 mL of dry DMSO. Yield 63 % as a white solid. ^{1}H NMR (600 MHz, DMSO-d_6) δ 14.18 (s, 1H), 8.38 (d, J = 8.5 Hz, 2H), 7.90 (d, J = 8.5 Hz, 2H), 7.20 (d, J = 9.0 Hz, 2H), 6.90 (d, J = 9.1 Hz, 2H), 3.90 – 3.81 (m, 2H), 3.50 (s, 3H), 3.25 – 3.14 (m, 4H), 3.13 – 2.99 (m, 4H), 1.65 – 1.50 (m, 2H), 0.88 (t, J = 7.4 Hz, 3H). ^{13}C NMR (151 MHz, DMSO-d_6) δ 154.6, 151.4, 149.6, 149.0, 148.2, 136.1, 133.4, 129.1, 128.8, 127.6, 123.7, 118.1, 109.1, 48.2, 46.1, 42.8, 30.3, 21.3, 11.7. HPLC-UV (254 nm) ESI-MS, purity: 97.3 %. LC-MS (m/z): 543 $[M + H]^+$. HRMS (ESI-TOF) m/z: $[M - H]^-$ calcd. for $C_{25}H_{27}ClN_6O_4S$ 541.1425, found 541.1425.

8-(4-((4-(4-Chlorophenyl)piperazin-1-yl)sulfonyl)phenyl)-3-ethyl-1-propyl-3,7-dihydropurine-2,6-dione (15) Method B. The compound was synthesized using **13c** (0.15 mmol) and 1-(4-chlorophenyl)piperazine (**55**, 0.225 mmol) in 4 mL of dry DMSO. Yield 58 % as a white solid. ^{1}H NMR (600 MHz, DMSO-d_6) δ 14.19 (s, 1H), 8.38 (d, J = 8.4 Hz, 2H), 7.90 (d, J = 8.4 Hz, 2H), 7.20 (d, J = 8.9 Hz, 2H), 6.90 (d, J = 9.0 Hz, 2H), 4.15 – 4.05 (m, 2H), 3.92 – 3.80 (m, 2H), 3.25 – 3.14 (m, 4H), 3.11 –3.00 (m, 4H), 1.65 – 1.53 (m, 2H), 1.27 (t, J = 7.0 Hz, 3H), 0.88 (t, J = 7.4 Hz, 3H). ^{13}C NMR (126 MHz, DMSO-d_6) δ 154.3, 150.5, 149.3, 148.1, 135.8, 133.1, 128.8, 128.5, 127.3, 123.4, 117.8, 112.8, 108.9, 47.9, 45.8, 42.4, 38.3, 21.0, 13.3, 11.3. HPLC-UV (254 nm) ESI-MS, purity: 97.4 %. LC-MS (m/z): 557 $[M + H]^+$. HRMS (ESI-TOF) m/z: $[M - H]^-$ calcd. for $C_{26}H_{29}ClN_6O_4S$ 555.1581, found 555.1604.

8-(4-((4-(4-Bromobenzyl)piperazin-1-yl)sulfonyl)phenyl)-1-propyl-3,7-dihydropurine-2,6-dione (16) Method B. The compound was synthesized using **13a** (0.15 mmol) and 1-(4-bromobenzyl)piperazine (**56**, 0.225 mmol) in 4 mL of dry DMSO. Yield 51 % as a white solid. ^{1}H

NMR (500 MHz, DMSO-d_6) δ 14.02 (br, 1H), 11.96 (br, 1H), 8.33 (d, J = 8.6 Hz, 2H), 7.84 (d, J = 8.6 Hz, 2H), 7.45 (d, J = 8.3 Hz, 2H), 7.18 (d, J = 8.3 Hz, 2H), 3.88 – 3.77 (m, 2H), 3.43 (s, 2H), 2.95 (br, 4H), 2.42 (br, 4H), 1.66 – 1.53 (m, 2H), 0.89 (t, J = 7.4 Hz, 3H). ^{13}C NMR (126 MHz, DMSO-d_6) δ 155.1, 151.1, 148.2, 147.7, 137.4, 135.8, 133.3, 131.2, 131.0, 128.4, 127.1, 120.1, 108.9, 60.5, 51.5, 46.1, 41.6, 40.3, 40.2, 40.1, 40.0, 40.0, 39.9, 39.7, 39.5, 39.4, 39.2, 21.0, 11.3. HPLC-UV (254 nm) ESI-MS, purity: 98.8 %. LC-MS (m/z): 587 $[M + H]^+$. HRMS (ESI-TOF) m/z: $[M – H]^–$ calcd. for $C_{25}H_{26}BrN_6O_4S$ 585.0920, found 585.0945.

8-(4-((4-(3-Bromobenzyl)piperazin-1-yl)sulfonyl)phenyl)-1-propyl-3,7-dihydropurine-2,6-dione (17) Method B. The compound was synthesized using **13a** (0.15 mmol) and 1-(3-bromobenzyl)piperazine (**57**, 0.225 mmol) in 4 mL of dry DMSO. Yield 54 % as a white solid. ^{1}H NMR (500 MHz, DMSO-d_6) δ 14.00 (br, 1H), 11.93(br, 1H), 8.33 (d, J = 8.6 Hz, 2H), 7.84 (d, J = 8.6 Hz, 2H), 7.44 – 7.37 (m, 2H), 7.26 – 7.21 (m, 2H), 3.86 – 3.78 (m, 2H), 3.46 (s, 2H), 2.96 (br, 4H), 2.43 (br, 4H), 1.59 (m, 2H), 0.89 (t, J = 7.4 Hz, 3H). ^{13}C NMR (126 MHz, DMSO-d_6) δ 155.1, 151.1, 148.2, 147.7, 140.9, 135.9, 133.3, 131.4, 130.5, 130.0, 128.4, 127.9, 127.1, 121.7, 119.9, 108.8, 60.6, 51.5, 46.1, 41.6, 21.0, 11.3. HPLC-UV (254 nm) ESI-MS, purity: 100 %. LC-MS (m/z): 587 $[M + H]^+$. HRMS (ESI-TOF) m/z: $[M – H]^–$ calcd. for $C_{25}H_{26}BrN_6O_4S$ 585.0920, found 585.0941.

8-(4-((4-(3-Methoxybenzyl)piperazin-1-yl)sulfonyl)phenyl)-1-propyl-3,7-dihydropurine-2,6-dione (18) Method B. The compound was synthesized using **13a** (0.15 mmol) and 1-(3-methoxybenzyl)piperazine (**58**, 0.225 mmol) in 4 mL of dry DMSO. Yield 31 % as a white solid. ^{1}H NMR (600 MHz, DMSO-d_6) δ 14.01 (br, 1H), 11.95 (br, 1H), 8.32 (d, J = 8.3 Hz, 2H), 7.83 (d, J = 8.3 Hz, 2H), 7.26 – 7.10 (m, 1H), 6.88 – 6.65 (m, 3H), 3.92 – 3.77 (m, 2H), 3.68 (s, 3H), 3.39 (s, 2H), 2.94 (s, 4H), 2.42 (s, 4H), 1.63 – 1.52 (m, 2H), 0.88 (t, J = 7.4 Hz, 3H). ^{13}C NMR (151

MHz, DMSO-d_6) δ 159.7, 155.4, 151.4, 148.5, 148.1, 139.8, 136.2, 133.5, 129.7, 128.7, 127.4, 121.3, 114.7, 112.9, 109.1, 61.8, 55.4, 51.9, 46.4, 42.0, 21.3, 11.7. HPLC-UV (254 nm) ESI-MS, purity: 97.3 %. LC-MS (m/z): 539 $[M + H]^+$. HRMS (ESI-TOF) m/z: $[M - H]^-$ calcd. for $C_{26}H_{30}N_6O_5S$ 537.1920, found 537.1919.

8-(4-((4-(3-Methylbenzyl)piperazin-1-yl)sulfonyl)phenyl)-1-propyl-3,7-dihydropurine-2,6-dione (19) Method B. The compound was synthesized using **13a** (0.15 mmol) and 1-(3-methylbenzyl)piperazine (**59**, 0.225 mmol) in 4 mL of dry DMSO. Yield 82 % as a white solid. ^{1}H NMR (500 MHz, DMSO-d_6) δ 11.82(br, 1H), 8.37 – 8.25 (m, 2H), 7.83 – 7.76 (m, 2H), 7.17 – 7.11 (m, 1H), 7.05 – 6.96 (m, 3H), 3.86 – 3.79 (m, 2H), 3.41 (s, 2H), 2.94 (br, 4H), 2.42 (br, 4H), 2.24 (s, 3H), 1.62 – 1.52 (m, 2H), 0.88 (t, J = 7.4 Hz, 3H). ^{13}C NMR (126 MHz, DMSO-d_6) δ 155.6, 151.2, 149.0, 148.0, 137.7, 137.4, 135.1, 129.5, 128.3, 128.2, 127.8, 126.8, 126.0, 61.6, 51.6, 46.1, 41.5, 21.1, 21.1, 11.3. HPLC-UV (254 nm) ESI-MS, purity: 98.6 %. LC-MS (m/z): 523 $[M + H]^+$. HRMS (ESI-TOF) m/z: $[M - H]^-$ calcd. for $C_{26}H_{29}N_6O_4S$ 521.1971, found 521.1984.

8-(4-((4-(4-Azidobenzyl)piperazin-1-yl)sulfonyl)phenyl)-1-propyl-3,7-dihydropurine-2,6-dione (20) Method A. The compound was synthesized using **13a** (0.15 mmol) and 1-(4-azidobenzyl)piperazine (**60**, 0.9 mmol) in 5 mL of DMF. Yield 33 % as an orange-brown solid. ^{1}H NMR (500 MHz, DMSO-d_6) δ 13.98 (br, 1H), 11.94 (br, 1H), 8.32 (d, J = 8.8 Hz, 2H), 7.83 (d, J = 8.9 Hz, 2H), 7.24 (d, J = 8.6 Hz, 2H), 6.99 (d, J = 8.5 Hz, 2H), 3.82 (t, J = 7.3 Hz, 3H), 3.43 (s, 2H), 2.94 (br, 4H), 2.48 (br, 4H), 1.70 – 1.49 (m, 2H), 0.89 (t, J = 7.6 Hz, 3H). ^{13}C NMR (126 MHz, DMSO-d_6) δ 155.1, 151.1, 148.1, 147.8, 138.1, 135.8, 134.8, 133.2, 130.5, 128.4, 127.1, 119.0, 60.7, 51.4, 46.1, 41.6, 21.0, 11.3. HPLC-UV (254 nm) ESI-MS, purity: 99 %. LC-MS (m/z): 550 $[M + H]^+$, 548 $[M - H]^-$.

8-(4-((4-(4-Carboxybenzyl)piperazin-1-yl)sulfonyl)phenyl)-1-propyl-3,7-dihydropurine-2,6-dione (21) Method C. ^{1}H NMR (500 MHz, DMSO-d_6) δ 13.37 (br, 1H), 11.98 (br, 1H), 8.32 (d, J = 8.8 Hz, 2H), 7.84 – 7.81 (m, 4H), 7.33 (d, J = 8.2 Hz, 2H), 3.82 (t, J = 7.3 Hz, 3H), 3.52 (s, 2H), 2.95 (br, 4H), 2.48 (br, 4H), 1.70 – 1.49 (m, 2H), 0.88 (t, J = 7.3 Hz, 3H). ^{13}C NMR (126 MHz, DMSO-d_6) δ 167.6, 155.3, 151.1, 148.4, 147.8, 143.0, 135.5, 133.8, 130.1, 129.4, 128.7, 128.4, 127.0, 109.5, 61.0, 51.7, 46.1, 41.6, 21.0, 11.3. HPLC-UV (254 nm) ESI-MS, purity: 98.0 %. LC-MS (m/z): 553 $[M + H]^+$, 551 $[M – H]^-$.

8-(4-((4-(4-(2-Hydroxyethoxy)benzyl)piperazine-1-yl)sulfonyl)phenyl)-1-propyl-3,7-dihydropurine-2,6-dione (22) Method B. The compound was synthesized using **13a** (0.15 mmol) and 2-(4-(piperazin-1-ylmethyl)phenoxy)ethanol (**62**, 0.9 mmol) in 2 mL of dry DMSO. Yield 5 % as a beige-colored solid. ^{1}H NMR (500 MHz, DMSO-d_6) δ: 13.94 (s, br,1H), 11.84 (s br, 1H), 8.29 (d, J = 8.5 Hz, 2H), 7.79 (d, J = 8.5 Hz, 2H), 7.08 (d, J = 8.7 Hz, 2H), 6.79 (d, J = 8.6 Hz, 2H), 4.76 (t, J = 5.4 Hz, 2H), 3.89 (t, J = 5.1 Hz, 2H), 3.95 – 3.76 (m, 8H), 3.66 (s, 2H), 3.64 (t, J = 5.2 Hz, 1H), 2.90 (s, 2H), 2.61 (m, 2H),1.57 – 1.53 (m, 2H), 0.86 (t, J = 7.4 Hz, 3H). ^{13}C NMR (125 MHz, DMSO-d_6) δ: 161.2, 157.9, 151.2, 148.1, 147.7, 136.0, 133.2, 130.1, 128.4, 127.0, 114.3, 108.0, 69.6, 60.9, 59.7, 51.5, 46.1, 40.6, 21.0, 11.3. HPLC-UV (254 nm) ESI-MS, purity: 97.6 %. LC-MS (m/z): 569 $[M + H]^+$.

8-(4-(4-((*p*-(2-(2-Methoxyethoxy)ethoxy)-phenyl)methyl)-1-piperazinylthio)phenyl)-1-3,7-dihydropurine-2,6-dione (23) Method A. The compound was synthesized by using **13a** (0.15 mmol) and 1-(2-methoxyethoxy)-2-(4-((1-piperazinyl)methyl)phenoxy) ethane (**63**, 0.9 mmol) in 5 mL of dry DMF. Yield 64 % as a yellowish solid. ^{1}H NMR (500 MHz, DMSO-d_6) δ: 14.00 (s, 1H), 11.94 (s, 1H), 8.31 (d, J = 8.5 Hz, 2H), 7.82 (d, J = 8.2 Hz, 2H), 7.09 (d, J = 8.5 Hz, 2H), 6.81 (d, J = 8.5 Hz, 2H), 4.00 - 4.02 (m, 2H), 3.81 - 3.84 (m, 2H), 3.68-3.69 (m, 2H), 3.54 - 3.56 (m, 2

H), 3.43 (t, *J* = 6.0 Hz, 2H), 3.37 (s, 2 H), 3.22 (s, 3 H), 2.92 (s, 4 H), 2.49 (s, 4 H), 1.57 (m, 2 H), 0.86 (t, *J* = 7.3 Hz, 3H).^{13}C NMR (150 MHz, DMSO-d_6) δ: 157.7, 155.1, 151.1, 148.2, 135.8, 133.2, 130.1, 129.7, 128.4, 127.1, 114.3,108.7, 71.4, 69.8, 69.1, 67.2, 60.8, 58.2, 51.4, 46.1, 39.2, 21.0,11.3. HPLC-UV (254 nm) ESI-MS, purity: 95.1 %. LC-MS (m/z): 627 $[M + H]^+$.

8-(4-((4-(3-Fluoro-4-methoxybenzyl)piperazin-1-yl)sulfonyl)phenyl)-1-propyl-3,7-dihydropurine-2,6-dione (24) Method B. The compound was synthesized using **13a** (0.15 mmol) and 1-(3-fluoro-4-methoxybenzyl)piperazine (**64**, 0.225 mmol) in 4 mL of dry DMSO. Yield 49 % as a withe solid. ^{1}H NMR (500 MHz, DMSO-d_6) δ 14.00 (br, 1H), 11.85 (br, 1H), 8.32 (d, *J* = 8.5 Hz, 2H), 7.82 (d, *J* = 8.5 Hz, 2H), 7.22 – 6.73 (m, 3H), 3.94 – 3.73 (m, 5H), 3.39 (s, 2H), 2.95 (br, 4H), 2.41 (br, 4H), 1.70 – 1.49 (m, 2H), 0.89 (t, *J* = 7.4 Hz, 3H). ^{13}C NMR (126 MHz, DMSO-d_6) δ 155.3, 152.4, 151.1, 150.5, 147.8, 146.3, 146.2, 135.5, 130.8, 128.3, 126.9, 125.0, 116.2, 116.0, 113.7, 109.5, 99.3, 92.5, 60.3, 56.1, 51.4, 46.1, 41.6, 21.0, 11.7. HPLC-UV (254 nm) ESI-MS, purity: 97.8 %. LC-MS (m/z): 557 $[M + H]^+$. HRMS (ESI-TOF) m/z: $[M - H]^-$ calcd. for $C_{26}H_{28}FN_6O_5S$ 555.1826, found 555.1826.

8-(4-((4-(4-Fluoro-3-methoxybenzyl)piperazin-1-yl)sulfonyl)phenyl)-1-propyl-3,7-dihydro-purine-2,6-dione (25) Method B. The compound was synthesized using **13a** (0.15 mmol) and 1-(4-fluoro-3-methoxybenzyl)piperazine (**65**, 0.225 mmol) in 4 mL of dry DMSO. Yield 45 % as a withe solid. ^{1}H NMR (500 MHz, DMSO-d_6) δ 14.01 (br, 1H), 11.94 (br, 1H), 8.33 (d, *J* = 8.3 Hz, 2H), 7.84 (d, *J* = 8.3 Hz, 2H), 7.07 (d, *J* = 10.0 Hz, 1H), 6.99 (d, *J* = 7.9 Hz, 1H), 6.77 (s, 1H), 3.89 – 3.78 (m, 2H), 3.75 (s, 3H), 3.42 (s, 2H), 2.95 (s, 4H), 2.42 (s, 4H), 1.63 – 1.51 (dd, *J* = 14.8, 7.4 Hz, 2H), 0.88 (t, *J* = 7.4 Hz, 3H). ^{13}C NMR (126 MHz, DMSO) δ 155.0, 151.1, 148.1, 147.8, 147.1, 147.0, 136.0, 134.6, 133.1, 128.4, 127.1, 121.0, 115.6, 114.2, 108.6, 94.7, 61.0, 56.0, 51.5, 46.0,

41.6, 21.0, 11.3. HPLC-UV (254 nm) ESI-MS, purity: 98.5 %. LC-MS (m/z): 557 $[M + H]^+$. HRMS (ESI-TOF) m/z: $[M - H]^-$ calcd. for $C_{26}H_{28}FN_6O_5S$ 555.1826, found 555.1835.

8-(4-((4-(3-Fluoro-5-methoxybenzyl)piperazin-1-yl)sulfonyl)phenyl)-1-propyl-3,7-dihydro-purine-2,6-dione (26) Method B. The compound was synthesized using **13a** (0.15 mmol) and 1-(3-fluoro-5-methoxybenzyl)piperazine (**66**, 0.225 mmol) in 4 mL of dry DMSO. Yield 42 % as a withe solid. ^{1}H NMR (500 MHz, DMSO-d_6) δ 14.00 (br, 1H), 11.92 (br, 1H), 8.48 – 8.18 (m, 2H), 7.83 (d, J = 8.6 Hz, 2H), 6.79 – 6.50 (m, 3H), 3.87 – 3.77 (m, 2H), 3.70 (s, 3H), 3.43 (s, 2H), 2.96 (s, 4H), 2.43 (s, 4H), 1.67 – 1.49 (m, 2H), 0.88 (t, J = 7.4 Hz, 3H). ^{13}C NMR (126 MHz, DMSO) δ 164.0, 162.1, 160.7, 155.2, 151.1, 148.2, 147.7, 141.5, 135.9, 133.4, 128.4, 127.1, 110.6, 107.2, 100.1, 60.9, 55.6, 51.6, 46.1, 41.6, 21.0, 11.3. HPLC-UV (254 nm) ESI-MS, purity: 100 %. LC-MS (m/z): 557 $[M + H]^+$. HRMS (ESI-TOF) m/z: $[M - H]^-$ calcd. for $C_{26}H_{28}FN_6O_5S$ 555.1826, found 555.1838.

8-(4-((4-(4-Bromo-3-fluorobenzyl)piperazin-1-yl)sulfonyl)phenyl)-1-propyl-3,7-dihydro-purine-2,6-dione (27) Method B. The compound was synthesized using **13a** (0.15 mmol) and 1-(3-fluoro-4-bromobenzyl)piperazine (**67**, 0.225 mmol) in 4 mL of dry DMSO. Yield 47 % as a withe solid. ^{1}H NMR (600 MHz, DMSO-d_6) δ 14.00 (br, 1H), 11.94 (br, 1H), 8.32 (d, J = 8.4 Hz, 2H), 7.83 (d, J = 8.3 Hz, 2H), 7.58 (t, J = 7.7 Hz, 1H), 7.22 (d, J = 9.8 Hz, 1H), 7.03 (d, J = 8.0 Hz, 1H), 3.89 – 3.75 (m, 2H), 3.46 (s, 2H), 2.95 (s, 4H), 2.43 (s, 4H), 1.64 – 1.48 (m, 2H), 0.88 (t, J = 7.4 Hz, 3H). ^{13}C NMR (151 MHz, DMSO) δ 159.4, 157.8, 155.5, 151.4, 148.2, 141.2, 141.1, 136.3, 133.6, 128.7, 127.4, 126.7, 117.1, 117.0, 106.6, 106.5, 60.4, 51.8, 46.4, 42.0, 21.4, 11.7. HPLC-UV (254 nm) ESI-MS, purity: 98.0 %. LC-MS (m/z): 605 $[M + H]^+$. HRMS (ESI-TOF) m/z: $[M - H]^-$ calcd. for $C_{25}H_{25}BrFN_6O_4S$ 603.0825, found 603.0830.

8-(4-((4-Phenylpiperazin-1-yl)sulfonyl)phenyl)-1-propyl-3,7-dihydropurine-2,6-dione (28) Method B. The compound was synthesized using **13a** (0.15 mmol) and 1-phenylpiperazine (**68**, 0.3 mmol) in 4 mL of dry DMSO. Yield 52 % as a withe solid. ^{1}H NMR (500 MHz, DMSO-d_6) δ 14.01 (s, 1H), 11.94 (s, 1H), 8.51 – 8.14 (m, 2H), 7.90 (d, J = 8.7 Hz, 2H), 7.37 – 7.05 (m, 2H), 6.96 – 6.84 (m, 2H), 6.81 – 6.76 (m, 1H), 3.83 (dd, J = 8.2, 6.7 Hz, 2H), 3.26 – 3.13 (m, 4H), 3.13 – 2.98 (m, 4H), 1.65 – 1.46 (m, 2H), 0.88 (t, 7.4 Hz, 3H). ^{13}C NMR (126 MHz, DMSO-d_6) δ 155.1, 151.1, 150.5, 148.1, 147.7, 135.7, 133.3, 129.1, 128.5, 127.1, 119.8, 116.3, 108.8, 48.1, 46.0, 41.6, 21.0, 11.3. HPLC-UV (254 nm) ESI-MS, purity: 95.6 %. LC-MS (m/z): 495 $[M + H]^+$. HRMS (ESI-TOF) m/z: $[M – H]^–$ calcd. for $C_{24}H_{25}N_6O_4S$ 493.1658, found 493.1699.

8-(4-((4-(4-Fluorophenyl)piperazin-1-yl)sulfonyl)phenyl)-1-propyl-3,7-dihydropurine-2,6-dione (29) Method B. The compound was synthesized using **13a** (0.15 mmol) and 1-(4-fluorophenyl)piperazine (**69**, 0.3 mmol) in 4 mL of dry DMSO. Yield 46 % as a withe solid. ^{1}H NMR (500 MHz, DMSO-d_6) δ 14.02 (br, 1H), 11.94 (s, 1H), 8.35 (d, J = 8.5 Hz, 2H), 7.90 (d, J = 8.5 Hz, 2H), 7.21 – 6.72 (m, 4H), 3.93 – 3.68 (m, 2H), 3.19 – 2.97 (m, 8H), 1.68 – 1.45 (m, 2H), 0.88 (t, J = 7.4 Hz, 3H). ^{13}C NMR (126 MHz, DMSO-d_6) δ 157.6, 155.7, 155.1, 151.1, 148.1, 147.4, 135.7, 133.3, 128.5, 127.1, 118.3, 118.2, 115.6, 115.4, 48.9, 46.0, 41.6, 21.0, 11.3. HPLC-UV (254 nm) ESI-MS, purity: 98.3 %. LC-MS (m/z): 513 $[M + H]^+$. HRMS (ESI-TOF) m/z: $[M – H]^–$ calcd. for $C_{24}H_{24}FN_6O_4S$ 511.1564, found 511.1584.

8-(4-((4-(3-Fluorophenyl)piperazin-1-yl)sulfonyl)phenyl)-1-propyl-3,7-dihydropurine-2,6-dione (30) Method B. The compound was synthesized using **13a** (0.15 mmol) and 1-(3-fluorophenyl)piperazine (**70**, 0.3 mmol) in 4 mL of dry DMSO. Yield 33 % as a withe solid. ^{1}H NMR (600 MHz, DMSO-d_6) δ 14.03 (br, 1H), 11.94 (br, 1H), 8.34 (d, J = 8.4 Hz, 2H), 7.89 (d, J = 8.4 Hz, 2H), 7.22 – 7.16 (m, 1H), 6.75 – 6.68 (m, 2H), 6.58 – 6.52 (m, 1H), 3.87 – 3.77 (m, 2H),

3.28 – 3.24 (m, 4H), 3.12 – 3.00 (m, 4H), 1.63 – 1.53 (m, 2H), 0.88 (t, *J* = 7.4 Hz, 3H). ^{13}C NMR (151 MHz, DMSO-d_6) δ 164.4, 162.8, 155.5, 152.6, 152.5, 151.4, 148.5, 148.1, 135.9, 133.8, 130.9, 130.8, 128.8, 127.5, 112.0, 106.1, 105.9, 103.1, 102.9, 47.9, 46.1, 42.0, 21.3, 11.7. HPLC-UV (254 nm) ESI-MS, purity: 95.5 %. LC-MS (m/z): 513 $[M + H]^+$. HRMS (ESI-TOF) m/z: $[M – H]^–$ calcd. for $C_{24}H_{24}FN_6O_4S$ 511.1564, found 511.1584.

8-(4-((4-(2-Fluorophenyl)piperazin-1-yl)sulfonyl)phenyl)-1-propyl-3,7-dihydropurine-2,6-dione (31) Method B. The compound was synthesized using **13a** (0.15 mmol) and 1-(2-fluorophenyl)piperazine (**71**, 0.3 mmol) in 4 mL of dry DMSO. Yield 21 % as a withe solid. ^{1}H NMR (600 MHz, DMSO-d_6) δ 14.03 (br, 1H), 11.94 (br, 1H), 8.31 (d, *J* = 8.4 Hz, 2H), 7.82 (d, *J* = 8.4 Hz, 2H), 7.11 – 7.07 (m, 2H), 7.06 – 7.01 (m, 1H), 7.00 – 6.94 (m, 1H), 3.83 – 3.79 (m, 2H), 3.12 – 3.05 (m, 8H), 1.59 – 1.53 (m, 2H), 0.88 (t, *J* = 7.4 Hz, 3H). ^{13}C NMR (126 MHz, DMSO-d_6) δ 151.4, 146.8, 140.0, 136.6, 128.7, 128.2, 126.5, 125.9, 119.9, 116.0, 100.1, 49.6, 46.2, 41.4, 21.2, 11.4. HPLC-UV (254 nm) ESI-MS, purity: 97.1 %. LC-MS (m/z): 513 $[M + H]^+$. HRMS (ESI-TOF) m/z: $[M – H]^–$ calcd. for $C_{24}H_{24}FN_6O_4S$ 511.1564, found 511.1567.

8-(4-{[4-(3-Chlorophenyl)piperazin-1-yl]sulfonyl}phenyl)-1-propyl-3,7-dihydropurine-2,6-dione (32) Method B. The compound was synthesized using **13a** (0.15 mmol) and 1-(3-chlorophenyl)piperazine (**72**, 0.3 mmol) in 4 mL of dry DMSO. Yield 29 % as a withe solid. ^{1}H NMR (500 MHz, DMSO-d_6) δ 13.98 (s, 1H), 11.93 (s, 1H), 8.34-8.39 (d, *J* = 8.50 Hz, 2H), 7.88 (d, *J* = 8.50, 2H), 7.17 (t, *J* = 8.1 Hz, 1H), 6.91 (t, *J* = 2.2 Hz, 1H), 6.83-6.87 (m, 1H), 6.77-6.80 (dd, 1H), 3.84 (t, 2H), 3.25 (s, 4H), 3.05 (s, 4H), 1.53-1.62 (m, 2H), 0.87 (t, *J* = 7.4 Hz, 3H). ^{13}C NMR (126 MHz, DMSO-d_6) δ 155.1, 155.7, 151.1, 148.1, 147.7, 135.7, 133.3, 130.6, 128.5, 127.2, 119, 115.5, 114.5, 47.5, 45.8, 41.6, 21, 11.3. HPLC-UV (254 nm) ESI-MS, purity: 98.2 %. LC-MS

(m/z): 529 $[M + H]^+$. HRMS (ESI-TOF) m/z: $[M – H]^–$ calcd. for $C_{24}H_{25}ClN_6O_4S$ 527.1347, found 527.1365.

8-(4-{[4-(2-Chlorophenyl)piperazin-1-yl]sulfonyl}phenyl)-1-propyl-3,7-dihydropurine-2,6-dione (33) Method B. The compound was synthesized using **13a** (0.15 mmol) and 1-(2-chlorophenyl)piperazine (**73**, 0.3 mmol) in 4 mL of dry DMSO. Yield 33 % as a withe solid. ^{1}H NMR (500 MHz, DMSO-d_6) δ 14.01 (s, 1H), 11.94 (s, 1H), 8.33-8.39 (d, J = 8.09 Hz, 2H), 7.90 (d, J = 8.50, 2H), 7.36 (d, J = 7.78 Hz, 1H), 7.27 (dd, J = 7.7 Hz, 1H), 7.15 (dd, J = 8.1 Hz, 1H), 7.03 (dd, J = 7.6 Hz, 1H), 3.84 (m, 2H), 3.13 (s, 4H), 3.05 (s, 4H), 1.56-1.60 (m, 2H), 1.23 (s,1H), 0.89 (t, J= 7.34 Hz, 3H). ^{13}C NMR (126 MHz, DMSO-d_6) δ 155.1, 151.1, 148.1, 147.7, 135.8, 133.3, 130.4, 128.5, 128.2, 127.8, 127.2, 124.7, 121.4, 108.7, 50.3, 46.4, 41.7, 21, 11.3. HPLC-UV (254 nm) ESI-MS, purity: 95.2 %. LC-MS (m/z): 529 $[M + H]^+$. HRMS (ESI-TOF) m/z: $[M – H]^–$ calcd. for $C_{24}H_{25}ClN_6O_4S$ 527.1347, found 527.1360.

8-(4-((4-(4-Bromophenyl)piperazin-1-yl)sulfonyl)phenyl)-1-propyl-3,7-dihydropurine-2,6-dione (34) Method B. The compound was synthesized using **13a** (0.15 mmol) and 1-(4-bromophenyl)piperazine (**74**, 0.3 mmol) in 4 mL of dry DMSO. Yield 67 % as a withe solid. ^{1}H NMR (500 MHz, DMSO-d_6) δ 13.94 (br, 1H), 11.91 (br, 1H), 8.34 (d, J = 8.6 Hz, 2H), 7.88 (d, J = 8.6 Hz, 2H), 7.35 – 7.27 (m, 2H), 6.91 – 6.80 (m, 2H), 3.86 – 3.79 (m, 2H), 3.24 – 3.18 (m, 4H), 3.10 – 3.00 (m, 4H), 1.68 – 1.47 (m, 2H), 0.88 (t, J = 7.4 Hz, 3H). ^{13}C NMR (126 MHz, DMSO-d_6) δ 155.1, 151.1, 149.6, 148.2, 147.7, 135.6, 133.5, 131.7, 128.4, 127.1, 118.2, 111.0, 109.0, 47.7, 45.8, 41.6, 21.0, 11.3. HPLC-UV (254 nm) ESI-MS, purity: 98.9 %. LC-MS (m/z): 575 $[M + H]^+$. HRMS (ESI-TOF) m/z: $[M – H]^–$ calcd. for $C_{24}H_{24}BrN_6O_4S$ 571.0763, found 571.0783.

8-(4-((4-(3-Bromophenyl)piperazin-1-yl)sulfonyl)phenyl)-1-propyl-3,7-dihydropurine-2,6-dione (35) Method B. The compound was synthesized using **13a** (0.15 mmol) and 1-(3-

bromophenyl)piperazine (**75**, 0.3 mmol) in 4 mL of dry DMSO. Yield 37 % as a withe solid. ^{1}H NMR (500 MHz, DMSO-d_6) δ 14.02 (s, 1H), 11.94 (s, 1H), 8.35 (d, J = 8.6 Hz, 2H), 7.89 (d, J = 8.5 Hz, 2H), 7.17 – 7.10 (m, 1H), 7.09 – 7.01 (m, 1H), 6.99 – 6.80 (m, 2H), 3.87 – 3.78 (m, 2H), 3.27 – 3.21 (m, 4H), 3.14 – 2.98 (m, 4H), 1.65 – 1.51 (m, 2H), 0.88 (t, J = 7.4 Hz, 3H). ^{13}C NMR (126 MHz, DMSO-d_6) δ 155.1, 151.9, 151.1, 148.1, 135.7, 133.4, 130.9, 128.5, 127.1, 122.6, 122.0, 118.3, 114.9, 108.7, 47.5, 45.8, 41.6, 21.0, 11.3. HPLC-UV (254 nm) ESI-MS, purity: 98.3 %. LC-MS (m/z): 575 $[M + H]^+$. HRMS (ESI-TOF) m/z: $[M - H]^-$ calcd. for $C_{24}H_{24}BrN_6O_4S$ 571.0818, found 571.0783.

8-(4-((4-(2-Bromophenyl)piperazin-1-yl)sulfonyl)phenyl)-1-propyl-3,7-dihydropurine-2,6-dione (36) Method B. The compound was synthesized using **13a** (0.15 mmol) and 1-(2-bromophenyl)piperazine (**76**, 0.3 mmol) in 4 mL of dry DMSO. Yield 43 % as a withe solid. ^{1}H NMR (500 MHz, DMSO-d_6) δ 14.02 (br, 1H), 11.94 (s, 1H), 8.37 (d, J = 8.5 Hz, 2H), 7.91 (d, J = 8.5 Hz, 2H), 7.61 – 7.50 (m, 1H), 7.39 – 7.28 (m, 1H), 7.22 – 7.13 (m, 1H), 7.03 – 6.94 (m, 1H), 3.92 – 3.66 (m, 2H), 3.18 – 2.92 (m, 8H), 1.66 – 1.52 (m, 2H), 0.89 (t, J = 7.4 Hz, 3H). ^{13}C NMR (126 MHz, DMSO-d_6) δ 155.1, 151.1, 149.6, 148.1, 135.7, 133.5, 133.4, 128.8, 128.4, 127.2, 125.4, 121.9, 119.2, 108.9, 50.7, 46.3, 41.6, 21.0, 11.3. HPLC-UV (254 nm) ESI-MS, purity: 97.8 %. LC-MS (m/z): 575 $[M + H]^+$. HRMS (ESI-TOF) m/z: $[M - H]^-$ calcd. for $C_{24}H_{24}BrN_6O_4S$ 571.0763, found 571.0783.

8-(4-((4-(4-Iodophenyl)piperazin-1-yl)sulfonyl)phenyl)-1-propyl-3,7-dihydropurine-2,6-dione (37) Method B. The compound was synthesized using **13a** (0.15 mmol) and 1-(4-iodophenyl)piperazine (**77**, 0.3 mmol) in 4 mL of dry DMSO. Yield 37 % as a withe solid. ^{1}H NMR (500 MHz, DMSO-d_6) δ 14.01 (br, 1H), 11.94 (s, 1H), 8.34 (d, J = 8.4 Hz, 2H), 7.89 (d, J = 8.5 Hz, 2H), 7.47 (d, J = 8.8 Hz, 2H), 6.74 (d, J = 8.9 Hz, 2H), 3.89 – 3.77 (m, 2H), 3.25 – 3.16 (m,

4H), 3.12 – 2.99 (m, 4H), 1.63 – 1.52 (m, 2H), 0.88 (t, *J* = 7.4 Hz, 3H). ^{13}C NMR (126 MHz, DMSO-d_6) δ 155.1, 151.1, 150.1, 148.1, 147.7, 137.5, 135.7, 133.3, 128.4, 127.1, 118.6, 108.8, 81.8, 47.6, 45.8, 41.6, 21.0, 11.3. LC/ESI-MS: negative mode m/z = ([M-H]$^-$), HPLC-UV (254 nm) ESI-MS, purity: 100.0 %. LC-MS (m/z): 621 $[M + H]^+$. HRMS (ESI-TOF) m/z: $[M – H]^–$ calcd. for $C_{24}H_{24}IN_6O_4S$ 619.0624, found 619.0694.

8-(4-((4-(4-Methoxyphenyl)piperazin-1-yl)sulfonyl)phenyl)-1-propyl-3,7-dihydropurine-2,6-dione (38) Method B. The compound was synthesized using **13a** (0.15 mmol) and 1-(3-methoxyphenyl)piperazine (**78**, 0.225 mmol) in 4 mL of dry DMSO. Yield 17 % as a withe solid. ^{1}H NMR (500 MHz, DMSO-d_6) δ 14.02 (s, 1H), 11.94 (s, 1H), 8.35 (d, *J* = 8.3 Hz, 2H), 7.89 (d, *J* = 8.3 Hz, 2H), 7.08 (t, *J* = 8.2 Hz, 1H), 6.61 – 6.21 (m, 3H), 3.87 – 3.77 (m, 2H), 3.68 (s, 3H), 3.25 – 3.15 (m, 4H), 3.12 – 2.98 (m, 4H), 1.71 – 1.46 (m, 2H), 0.88 (t, *J* = 7.4 Hz, 3H). ^{13}C NMR (126 MHz, DMSO-d_6) δ 160.3, 155.1, 151.8, 151.1, 148.1, 147.7, 135.7, 133.3, 129.8, 128.5, 127.2, 108.8, 108.7, 105.1, 102.5, 55.0, 48.1, 45.9, 41.6, 21.0, 11.3. HPLC-UV (254 nm) ESI-MS, purity: 97.6 %. LC-MS (m/z): 525 $[M + H]^+$. HRMS (ESI-TOF) m/z: $[M – H]^–$ calcd. for $C_{25}H_{27}N_6O_5S$ 523.1764, found 523.1773.

8-(4-((4-(4-Methylphenyl)piperazin-1-yl)sulfonyl)phenyl)-1-propyl-3,7-dihydropurine-2,6-dione (39) Method B. The compound was synthesized using **13a** (0.15 mmol) and 1-(*p*-tolyl)piperazine (**79**, 0.225 mmol) in 4 mL of dry DMSO. Yield 25 % as a withe solid. ^{1}H NMR (500 MHz, DMSO-d_6) δ 14.00 (br, 1H), 11.94 (s, 1H), 8.35 (d, *J* = 8.5 Hz, 2H), 7.89 (d, *J* = 8.5 Hz, 2H), 7.00 (d, *J* = 8.4 Hz, 2H), 6.79 (d, *J* = 8.5 Hz, 2H), 3.91 – 3.74 (m, 2H), 3.20 – 2.96 (m, 8H), 2.19 (s, 3H), 1.68 – 1.49 (m, 2H), 0.88 (t, *J* = 7.4 Hz, 3H). ^{13}C NMR (126 MHz, DMSO-d_6) δ 155.1, 151.1, 148.4, 148.1, 147.7, 135.7, 133.3, 129.5, 128.8, 128.4, 127.1, 116.6, 108.8, 48.6, 46.0,

41.6, 21.0, 20.1, 11.3. HPLC-UV (254 nm) ESI-MS, purity: 98.1 %. LC-MS (m/z): 509 $[M + H]^+$. HRMS (ESI-TOF) m/z: $[M - H]^-$ calcd. for $C_{25}H_{27}N_6O_4S$ 507.1814, found 507.1823.

1-Propyl-8-(4-((4-(o-tolyl)piperazin-1-yl)sulfonyl)phenyl)-1-propyl-3,7-dihydropurine-2,6-dione (40) Method B. The compound was synthesized using **13a** (0.15 mmol) and 1-(*o*-tolyl)piperazine (**80**, 0.225 mmol) in 4 mL of dry DMSO. Yield 30 % as a withe solid. ^{1}H NMR (500 MHz, DMSO-d_6) δ 14.02 (s, 1H), 11.95 (s, 1H), 8.37 (d, J = 8.4 Hz, 2H), 7.91 (d, J = 8.5 Hz, 2H), 7.03 (dq, J = 36.0, 7.4 Hz, 4H), 3.91 – 3.75 (m, 2H), 3.10 (s, 4H), 2.90 (d, J = 4.2 Hz, 4H), 2.11 (s, 3H), 1.59 (dd, J = 14.8, 7.3 Hz, 2H), 0.89 (t, J = 7.4 Hz, 3H). ^{13}C NMR (126 MHz, DMSO-d_6) δ 155.1, 151.1, 150.6, 148.1, 147.7, 136.0, 133.3, 132.1, 131.0, 128.4, 127.2, 126.7, 123.6, 119.3, 108.8, 50.8, 46.6, 41.6, 21.0, 17.6, 11.3. HPLC-UV (254 nm) ESI-MS, purity: 98.5 %. LC-MS (m/z): 509 $[M + H]^+$. HRMS (ESI-TOF) m/z: $[M - H]^-$ calcd. for $C_{25}H_{27}N_6O_4S$ 507.1814, found 507.1813.

8-(4-((4-(4-Hydroxyphenyl)piperazine-1-yl)sulfonyl)phenyl)-1-propyl-3,7-dihydropurine-2,6-dione (41) Method C. ^{1}H NMR (600 MHz, DMSO-d_6) δ 14.05 (s, 1H), 11.97 (s, 1H), 8.36 (d, J = 8.6 Hz, 2H), 7.90 (d, J = 8.6 Hz, 2H), 6.97 (s, 2H), 6.68 (d, J = 8.4 Hz, 2H), 3.86 – 3.79 (m, 2H), 3.68 (s, 4H), 3.17 (s, 4H), 1.63 – 1.53 (m, 2H), 0.88 (t, J = 7.4 Hz, 3H). ^{13}C NMR (150 MHz, DMSO-d_6) δ 155.4, 151.4, 148.3, 148.0, 135.8, 133.7, 128.9, 127.5, 120.4, 116.1, 109.1, 51.4, 45.8, 42.0, 21.3, 11.7. HPLC-UV (254 nm) ESI-MS, purity: 98.4 %. LC-MS (m/z): 511 $[M + H]^+$. HRMS (ESI-TOF) m/z: $[M - H]^-$ calcd. for $C_{24}H_{25}N_6O_5S$ 509.1607, found 509.1622.

8-(4-((4-Benzoylpiperazin-1-yl)sulfonyl)phenyl)-1-propyl-3,7-dihydropurine-2,6-dione (42) Method B. The compound was synthesized using **13a** (0.15 mmol) and phenyl(piperazin-1-yl)methanone (**82**, 0.225 mmol) in 4 mL of dry DMSO. Yield 37 % as a withe solid. ^{1}H NMR (500 MHz, DMSO-d_6) δ 14.00 (br, 1H), 11.96 (s, 1H), 8.35 (d, J = 8.7 Hz, 2H), 7.87 (d, J = 8.7 Hz, 2H),

7.47 – 7.31 (m, 5H), 3.90 – 3.80 (m, 2H), 3.52 (br, 4H), 3.04 (br, 4H), 1.60 (dd, *J* = 14.9, 7.4 Hz, 2H), 0.89 (t, *J* = 7.5 Hz, 3H). ^{13}C NMR (126 MHz, DMSO-d_6) δ 169.3, 155.1, 151.1, 147.8, 136.0, 135.4, 133.3, 129.8, 128.5, 128.3, 127.1, 112.0, 45.8, 41.6, 40.3, 21.0, 11.3. HPLC-UV (254 nm) ESI-MS, purity: 98.0 %. LC-MS (m/z): 523 $[M + H]^+$. HRMS (ESI-TOF) m/z: $[M – H]^–$ calcd. for $C_{25}H_{25}N_6O_5S$ 521.1607, found 521.1614.

8-(4-((4-(1-Phenylethyl)piperazin-1-yl)sulfonyl)phenyl)-1-propyl-3,7-dihydropurine-2,6-dione (43) Method B. The compound was synthesized using **13a** (0.15 mmol) and 1-(1-phenylethyl)piperazine (**83**, 0.225 mmol) in 4 mL of dry DMSO. Yield 41 % as a withe solid. ^{1}H NMR (600 MHz, DMSO-d_6) δ 13.91 (br, 1H), 11.88 (br, 1H), 8.32 (d, *J* = 8.5 Hz, 2H), 7.81 (d, *J* = 8.5 Hz, 2H), 7.29 – 7.15 (m, 5H), 3.89 – 3.75 (m, 2H), 3.45 – 3.39 (m, 1H), 2.97 – 2.84 (m, 4H), 2.48 – 2.43 (m, 2H), 2.40 – 2.32 (m, 2H), 1.64 – 1.54 (m, 2H), 1.22 (d, *J* = 6.7 Hz, 3H), 0.89 (t, *J* = 7.4 Hz, 3H). ^{13}C NMR (151 MHz, DMSO-d_6) δ 155.7, 151.5, 148.2, 143.4, 128.7, 128.6, 127.8, 127.3, 127.3, 63.5, 49.2, 46.7, 41.9, 40.6, 21.4, 19.4, 11.7. HPLC-UV (254 nm) ESI-MS, purity: 96.8 %. LC-MS (m/z): 523 $[M + H]^+$. HRMS (ESI-TOF) m/z: $[M – H]^–$ calcd. for $C_{26}H_{29}N_6O_4S$ 521.1971, found 521.1984.

8-(4-((4-Methylpiperazin-1-yl)sulfonyl)phenyl)-1-propyl-3,7-dihydropurine-2,6-dione (44) Method B. The compound was synthesized using **13a** (0.15 mmol) and 1-methylpiperazine (**84**, 0.225 mmol) in 4 mL of dry DMSO. Yield 37 % as a withe solid. ^{1}H NMR (500 MHz, DMSO-d_6) δ 13.91 (br, 1H), 11.88 (br, 1H), 8.51 – 8.16 (m, 2H), 7.94 – 7.75 (m, 2H), 3.95 – 3.75 (m, 2H), 2.94 (s, 4H), 2.42 – 2.31 (m, 4H), 2.14 (s, 3H), 1.58 (dt, *J* = 14.8, 7.4 Hz, 2H), 0.88 (t, *J* = 7.4 Hz, 3H). ^{13}C NMR (126 MHz, DMSO-d_6) δ 155.2, 151.1, 148.4, 147.8, 135.7, 133.6, 128.3, 127.0, 53.6, 45.9, 45.4, 41.6, 21.0, 11.3. HPLC-UV (254 nm) ESI-MS, purity: 99.1 %. LC-MS (m/z): 433 $[M + H]^+$. HRMS (ESI-TOF) m/z: $[M – H]^–$ calcd. for $C_{19}H_{23}N_6O_4S$ 431.1501, found 431.1519.

8-(4-({[4-(3-Fluoro-4-methoxyphenyl)piperazin-1-yl]sulfonyl}phenyl)-1-propyl-3,7-dihydropurine-2,6-dione (45) New approach. Yield 41 % as a withe solid.^{1}H NMR (500 MHz, DMSO-d_6) δ 13.95 (s, 1H), 11.91 (s, 1H), 8.33 (d, J = 8.51 Hz, 2H), 7.88 (d, J = 8.70 Hz, 2H), 6.98 (d, J = 9.98, 1H), 6.82 (d, J = 14.32 Hz, 1H), 6.63 (dd, J = 9.07 Hz, 1H), 3.78-3.85 (m, 2H), 3.72 (s, 3H), 3.10-3.13 (m, 4H), 3.05 (m, 4H), 1.52-1.62 (m, 2H), 0.87 (t, J= 7.43 Hz, 3H). ^{13}C NMR (126 MHz, DMSO-d_6) δ 155.2, 153, 151.1, 148.2, 145.2, 140.9, 135.6, 133.5, 128.4, 127.1, 114.9, 112.1, 105.7, 105.5, 56.6, 48.8, 45.9, 41.6, 21, 11.3. HPLC-UV (254 nm) ESI-MS, purity: 95.8 %. LC-MS positive mode (m/z): 542 $[M + H]^+$. HRMS (ESI-TOF) m/z: $[M - H]^-$ calcd. for $C_{25}H_{27}FN_6O_5S$ 541.1748, found 541.1679.

8-(4-{[4-(3-Chloro-4-methoxyphenyl)piperazin-1-yl]sulfonyl}phenyl)-1-propyl-3,7-dihydropurine-2,6-dione (46) New approach. Yield 10 % as a withe solid. ^{1}H NMR (500 MHz, DMSO-d_6) δ 14 (s, 1H), 11.93 (s, 1H), 8.34 (d, J = 8.70 Hz, 2H), 7.88 (d, J = 8.80, 1H), 6.98 (d, J = 7.75 Hz, 1H), 6.84 (dd, J = 8.95 Hz, 1H), 3.75-3.85 (t, J = 8.89 Hz, 2H), 3.74 (s, 3H), 3.10-3.13 (m, 4H), 3.01-3.09 (m, 4H), 1.50-1.60 (m, 2H), 0.87 (t, J= 7.16 Hz, 3H). ^{13}C NMR (126 MHz, DMSO-d_6) δ 155, 151.1, 148.7, 145.3, 133.3, 128.4, 127.1, 121.6, 118.6, 116.5, 113.7, 56.4, 49, 46, 41.6, 21, 11.3. HPLC-UV (254 nm) ESI-MS, purity: 96.6 %. LC-MS (m/z): 559 $[M + H]^+$. HRMS (ESI-TOF) m/z: $[M - H]^-$ calcd. for $C_{25}H_{27}ClN_6O_5S$ 557.1452, found 557.1391.

8-(4-{[4-(4-Chloro-3-methoxyphenyl)piperazin-1-yl]sulfonyl}phenyl)-1-propyl-3,7-dihydropurine-2,6-dione (47) New approach. Yield 58 % as a withe solid. ^{1}H NMR (500 MHz, DMSO-d_6) δ 14.01 (s, 1H), 11.93 (s, 1H), 8.34 (d, J = 8.70 Hz, 2H), 7.84-7.89 (d, J = 8.70 Hz, 2H), 7.16 (d, J = 8.80, 1H), 6.62 (d, J = 2.60 Hz, 1H), 6.44 (dd, J = 8.80 Hz, 1H), 3.75-3.85 (t, J = 8.30 Hz, 2H), 3.78 (s, 3H), 3.20-3.26 (m, 4H), 3.01-3.09 (m, 4H), 1.50-1.60 (m, 2H), 0.87 (t, J = 8.7 Hz, 3H). ^{13}C NMR (126 MHz, DMSO-d_6) δ 155, 151, 150.8, 135.7, 133.3, 129.8, 128.5, 127.1,

111.8, 108.8, 101.8, 56, 48.1, 45.9, 41.6, 21, 11.3. HPLC-UV (254 nm) ESI-MS, purity: 96.6 %. LC-MS positive mode (m/z): 559 $[M + H]^+$. HRMS (ESI-TOF) m/z: $[M - H]^-$ calcd. for $C_{25}H_{27}ClN_6O_5S$ 557.1452, found 557.1385.

8-(4-{[4-(3-Chloro-4-hydroxyphenyl)piperazin-1-yl]sulfonyl}phenyl)-1-propyl-3,7-dihydropurine-2,6-dione (48) New approach. Yield 25 % as a withe solid.^{1}H NMR (500 MHz, DMSO-d_6) δ 11.91 (s, 1H), 9.49 (s, 1H), 8.33 (d, J = 8.30 Hz, 2H), 7.84-7.89 (d, J = 8.20 Hz, 2H), 6.86 (d, J = 8.80, 1H), 6.81 (d, J = 8.90 Hz, 1H), 6.73 (dd, J = 8.80 Hz, 1H), 3.82-3.85 (t, J = 8.30 Hz, 2H), 3.01-3.09 (m, 8H), 1.50-1.65 (m, 2H), 0.87 (t, J= 7.4 Hz, 3H). ^{13}C NMR (126 MHz, DMSO-d_6) δ 155.2, 151.1, 148.3, 148, 147.1, 144.3, 135.5, 133.6, 128.4, 127.1, 119.9, 118.5, 117.4, 117.1, 49.3, 46.1, 41.6, 21, 11.3. HPLC-UV (254 nm) ESI-MS, purity: 99.0 %. LC-MS (m/z): 545 $[M + H]^+$. HRMS (ESI-TOF) m/z: $[M - H]^-$ calcd. for $C_{24}H_{25}ClN_6O_5S$ 543.1296, found 543.1233.

8-(4-{[4-(4-Chloro-3-hydroxyphenyl)piperazin-1-yl]sulfonyl}phenyl)-1-propyl-3,7-dihydropurine-2,6-dione (49) New approach. Yield 13 % as a withe solid. ^{1}H NMR (500 MHz, DMSO-d_6) δ 11.86 (s, 1H), 9.86 (s, 1H), 8.32 (d, J = 6.10 Hz, 2H), 7.84-7.89 (d, J = 8.60 Hz, 2H), 7.08 (d, J = 8.80, 1H), 6.43-6.47 (d, J = 2.60 Hz, 1H), 6.32-6.39 (dd, J = 8.80 Hz, 1H), 3.62-3.87 (t, J = 8.30 Hz, 2H), 3.10-3.20 (m, 4H), 3.01-3.09 (m, 4H), 1.47-1.65 (m, 2H), 0.87 (t, J = 8.5 Hz, 3H). ^{13}C NMR (126 MHz, DMSO-d_6) δ 155.33, 153.4, 151.1, 150.5, 147.8, 129.8, 128.4, 127, 110.6, 108.6, 104.4, 48, 45.9, 41.6, 21, 11.3. HPLC-UV (254 nm) ESI-MS, purity: 95.0 %. LC-MS (m/z): 545 $[M + H]^+$. HRMS (ESI-TOF) m/z: $[M - H]^-$ calcd. for $C_{24}H_{25}ClN_6O_5S$ 543.1296, found 543.1268.

8-(4-((4-(4-Chloro-2-fluorophenyl)piperazin-1-yl)sulfonyl)phenyl)-1-propyl-3,7-dihydropurine-2,6-dione (50) Method B. The compound was synthesized using **13a** (0.15 mmol) and 1-(4-chloro-2-fluorophenyl)piperazine (**88**, 0.3 mmol) in 4 mL of dry DMSO. Yield 82 % as a

withe solid. ^{1}H NMR (600 MHz, DMSO-d_6) δ 14.01 (br, 1H), 11.93 (br, 1H), 8.35 (d, J = 8.6 Hz, 2H), 7.89 (d, J = 8.6 Hz, 2H), 7.33 – 7.28 (m, 1H), 7.19 – 3.15 (m, 1H), 7.07 – 7.05 (m, 1H), 3.87 – 3.77 (m, 2H), 3.09 (s, 8H), 1.70 – 1.47 (m, 2H), 0.88 (t, J = 7.4 Hz, 3H). ^{13}C NMR (151 MHz, DMSO-d_6) δ 155.7, 151.4, 148.5, 138.6, 136.0, 128.8, 127.5, 125.3, 121.4, 117.1, 49.8, 46.4, 42.0, 21.3, 11.7. HPLC-UV (254 nm) ESI-MS, purity: 97.4 %. LC-MS (m/z): 547 $[M + H]^+$. HRMS (ESI-TOF) m/z: $[M – H]^–$ calcd. for $C_{24}H_{23}ClFN_6O_4S$ 545.1174, found 545.1196.

8-(4-((4-(4-(2-Hydroxyethoxy)phenyl)piperazine-1-yl)sulfonyl)phenyl)-1-propyl-3,7-dihydropurine-2,6-dione (**51**) Method B. The compound was synthesized using **13a** (0.15 mmol) and 1-(4-(2-hydroxyethoxy)phenyl))piperazine (**89**, 0.3 mmol) in 4 mL of dry DMSO. Yield 18 % as a beige-colored solid. ^{1}H NMR (500 MHz, DMSO-d_6) δ: 11.91 (s, br, 1H), 8.34 (d, J = 8.5 Hz, 2H), 7.87 (d, J = 8.5 Hz, 2H), 6.86 – 6.76 (m, 4H, CH), 4.76 (m, 2H), 3.87 (t, J = 5.1 Hz, 2H), 3.84 – 3.79 (t, J = 7.4 Hz, 2H), 3.64 (s br, 1H), 3.06 (s, 8H), 1.57 (m, 2H), 0.87 (t, J = 7.4 Hz, 3H). ^{13}C NMR (125 MHz, DMSO-d_6) δ: 155.3, 153.1, 151.1, 148.4, 147.8, 144.8, 135.5, 133.8, 128.4, 127.1, 118.4, 115.2, 69.9, 59.8, 49.5, 46.1, 41.6, 21.0, 11.3. HPLC-UV (254 nm) ESI-MS, purity: 98.4 %. LC-MS (m/z): 555 $[M + H]^+$.

8-(4-((4-Methyl-3-phenylpiperazin-1-yl)sulfonyl)phenyl)-1-propyl-3,7-dihydropurine-2,6-dione (52) Method B. The compound was synthesized using **13a** (0.15 mmol) and 1-methyl-2-phenylpiperazine (**90**, 0.225 mmol) in 4 mL of dry DMSO. Yield 77 % as a withe solid. ^{1}H NMR (500 MHz, DMSO-d_6) δ 14.00 (br, 1H), 11.93 (br, 1H), 8.31 (d, J = 8.5 Hz, 2H), 7.84 (d, J = 8.5 Hz, 2H), 7.59 – 7.05 (m, 5H), 3.86 – 3.80 (m, 2H), 3.71 – 3.65 (m, 1H), 3.44 – 3.40 (m, 1H), 3.11 – 3.06 (m, 1H), 3.00 – 2.95 (m, 1H), 2.55 – 2.51 (m, 1H), 2.32 – 2.27 (m, 1H), 2.19 – 2.24 (m, 1H), 1.91 (s, 3H), 1.67 – 1.51 (m, 2H), 0.88 (t, J = 7.4 Hz, 3H). ^{13}C NMR (126 MHz, DMSO-d_6) δ 155.2, 151.1, 148.2, 145.7, 140.0, 139.3, 135.8, 133.4, 132.4, 132.3, 128.8, 128.4, 128.1, 127.8, 127.1,

109.0, 67.3, 54.1, 52.5, 46.1, 42.7, 41.6, 21.0, 11.3. HPLC-UV (254 nm) ESI-MS, purity: 95.9 %. LC-MS (m/z): 509 $[M + H]^+$. HRMS (ESI-TOF) m/z: $[M - H]^-$ calcd. for $C_{25}H_{27}N_6O_4S$ 507.1814, found 507.1833.

4-(2,6-Dioxo-1-propyl-2,3,6,7-tetrahydro-purin-8-yl)-*N*,*N*-dimethylbenzenesulfonamide (53) Method D. Yield 29 % as a beige-colored solid. ^{1}H NMR (500 MHz, DMSO-d_6) δ 13.82 (br, 1H), 11.96 (br, 1H), 8.38 – 8.26 (m, 2H), 7.97 – 7.62 (m, 2H), 3.89 – 3.74 (m, 2H), 2.65 (s, 6H), 1.66 – 1.50 (m, 2H), 0.88 (t, J = 7.4 Hz, 3H). ^{13}C NMR (126 MHz, DMSO-d_6) δ 155.3, 151.1, 148.5, 147.8, 135.5, 133.6, 128.3, 126.9, 109.4, 41.6, 37.7, 21.0, 11.3. HPLC-UV (254 nm) ESI-MS, purity: 95.9 %. LC-MS (m/z): 378 $[M + H]^+$. HRMS (ESI-TOF) m/z: $[M - H]^-$ calcd. for $C_{16}H_{19}N_5O_4S$ 376.1079, found 376.1112.

4-(2,6-Dioxo-1-propyl-2,3,6,7-tetrahydro-purin-8-yl)-*N*-methyl-*N*-phenethylbenzenesulfonamide (54) Method B. The compound was synthesized using **13a** (0.15 mmol) and N-methyl-2-phenylethan-1-amine (**92**, 0.225 mmol) in 4 mL of dry DMSO. Yield 63 % as a withe solid. ^{1}H NMR (600 MHz, DMSO-d_6) δ 13.98 (br, 1H), 11.92 (br, 1H), 8.41 – 8.10 (m, 2H), 7.86 (d, J = 8.6 Hz, 2H), 7.38 – 7.04 (m, 5H), 3.84 – 3.81 (m, 2H), 3.27 – 3.20 (m, 2H), 2.84 – 2.78 (m, 2H), 2.73 (s, 3H), 1.76 – 1.47 (m, 2H), 0.88 (t, J = 7.4 Hz, 3H). ^{13}C NMR (151 MHz, DMSO-d_6) δ 151.4, 138.9, 129.2, 128.8, 128.3, 127.4, 126.8, 116.9, 115.0, 51.5, 41.9, 40.6, 40.4, 40.3, 40.2, 40.0, 39.9, 39.8, 39.6, 35.2, 34.1, 21.3, 11.7. HPLC-UV (254 nm) ESI-MS, purity: 99.1 %. LC-MS (m/z): 468 $[M + H]^+$. HRMS (ESI-TOF) m/z: $[M - H]^-$ calcd. for $C_{16}H_{19}N_5O_4S$ 466.1549, found 466.1555.

1.4 Water solubility

Semi-thermodynamic solubility was determined by the shaking flask method (Pharmacelsus, Saarbrücken, Germany). Test compounds were dissolved in DMSO (20 mM). This stock solution was used to spike 3 tubes containing phosphate-buffered saline (cut-off concentration 200 μM) with a final concentration of 1 % DMSO. Tubes were shaken for 24 h, undissolved particles were removed by centrifugation and the supernatant was used for quantification by LC/MS using a 5-8 point calibration curve.

2. Biological assays

2.1 Membrane preparation

Membrane preparations of recombinant CHO or HEK cells stably expressing human or mouse AR subtypes were conducted as previously described,[32] or purchased from Perkin Elmer (Solingen, Germany).

2.2 Radioligand receptor binding assays

[^{3}H]2-Chloro-N^6-cyclopentyladenosine ([^{3}H]CCPA, A_1) (1 nM), [^{3}H](*E*)-3-(3-hydroxypropyl)-8-(2-(*m*-methoxyphenyl)vinyl)-7-methyl-1-prop-2-ynyl-3,7-dihydropurine-2,6-dione ([^{3}H]MSX-2, A_{2A}) (1 nM), [^{3}H]8-(4-(4-(4-chlorophenyl)piperazine-1-sulfonyl)phenyl)-1-propyl-3,7-dihydropurine-2,6-dione ([^{3}H]PSB-603, A_{2B}) (0.3 nM), and [^{3}H]2-phenyl-8-ethyl-4-methyl-(8*R*)-4,5,7,8-tetrahydro-1*H*-imidazo[2.1-*i*]purin-5-one ([^{3}H]PSB-11, A_3) (1 nM) were used as radioligands for human and mouse A_1, A_{2A}, A_{2B}, and human A_3AR, respectively. [^{3}H]NECA (10 nM) was used as a radioligand for the mouse A_3AR.

Competition binding experiments at human and mouse A_1, A_{2A}, and A_3 ARs were performed in a final volume of 400 μL containing 4 μL of test compound dissolved in DMSO, 196 μL buffer (50

mM Tris-HCl, pH 7.4; mouse A_3: 50 mM Tris-HCl, 10 mM $MgCl_2$, pH 7.4), 100 μL of radioligand solution in the same buffer and 100 μL of membrane preparation (5-100 μg protein per vial, 2 U/mL adenosine deaminase (ADA), preincubation for 15 min at rt). Competition binding experiments at human and mouse A_{2B}ARs were performed in a final volume of 1 mL containing 10 μL of test compound dissolved in 100 % DMSO, 790 μL buffer (50 mM Tris-HCl, pH 7.4), 100 μL of radioligand solution in the same buffer, and 100 μL of membrane preparation (10-100 μg protein per vial, 2 U/mL ADA, preincubationfor 15 min at rt). Non-specific binding was determined in the presence of 2-chloroadenosine (10 μM f. c.), CGS-15943 (10 μM f. c.), DPCPX (10 μM f. c.) or *R*-PIA (100 μM f. c.) for human and mouse A_1, A_{2A}, A_{2B}, and A_3AR, respectively. The incubation time at rt was 90 min for A_1ARs, 30 min for A_{2A}ARs, 75 min for A_{2B}ARs, 45 min for human A_3ARs with the radioligand [^{3}H]PSB-11, and 180 min for the mouse A_3AR using the radioligand [^{3}H]NECA. After the incubation, the assay mixture was filtered through GF/B glass fiber filters using a Brandel harvester (Brandel, Gaithersburg, MD). Filters were washed three times (3 - 4 mL each) with ice-cold 50 mM Tris-HCl buffer, pH 7.4. For the A_{2A}AR assay the GF/B glass fiber filters were preincubated for 30 min in 0.3 % aq. polyethylenemine solution. The GF/B glass fiber filters for the A_{2B}AR assays were washed four times (3 - 4 mL each) with ice-cold 50 mM Tris-HCl buffer, pH 7.4 containing 0.1 % BSA in order to reduce non-specific binding. Then filters were transferred to vials, incubated for 9 h with 2.5 mL of scintillation cocktail (Luma Safe, Perkin Elmer), and counted in a liquid scintillation counter (Tri-Carb 2810 TR) with a counting efficiency of ~52 %. Three to four separate experiments were performed for the determination of K_i values. All data were analyzed with GraphPad Prism, Version 4.1 (GraphPad Inc., La Jolla, CA).

2.3 cAMP accumulation assays

cAMP accumulation assays were conducted as described before[32, 52] with some modifications. For antagonist testing 50 μL of different dilutions of antagonist in Hank's Balanced Salt Solution (HBSS) containing 5 % DMSO were added and the cells were incubated for 10 min at 37 °C and 5 % CO_2. Then 50 μL of various dilutions of the agonist NECA (Sigma) in HBSS containing 5 % DMSO were added and the cells were incubated for 15 min under the same conditions as described above. As an internal assay control and for standardization, 50 μL of 5 % DMSO/95 % HBSS buffer and 50 μL of forskolin (final concentration 10 μM) in HBSS containing 5 % DMSO were added to the cells and incubated for 15 min at 37 °C and 5 % CO_2. Three to four separate experiments were performed for the determination of EC_{50} values, each in duplicates or triplicates. All other assay conditions were performed as described previously.[32]

3. Homology modeling and docking studies

3.1 Homology modeling

A homology model of the human A_{2B}AR using Modeller9 was generated based on the high resolution (1.8 Å) crystal structure of the human A_{2A}AR. [63, 68, 69] The entry 4EIY.pdb was downloaded from the Protein Data Bank and used as a template, in which the human A_{2A}AR receptor was crystallized in complex with an antagonist, ZM241385.[63] The sequence of the human A_{2B}AR with the accession number of P29275 was retrieved from the UniProt sequence database (http:// http://www.uniprot.org/). A sequence similarity of 73.1 % and an identity of 58.3 % between the human A_{2B}AR and the human A_{2A}AR justified the choice of this structure as a template for the homology model. The sequences were aligned using the alignment tool Clustal Omega.[70] The resulted alignment was used as input to the Modeller9 program, and each model was optimized using the variable target function method (VTFM). From the 100 generated models, the Discrete Optimized Protein Energy (DOPE) score included in Modeller was utilized to select the best model

of the human $A_{2B}AR$.[69] The overall structural quality was confirmed by a Ramachandran Plot, and sequence-structure compatibility of the model was ensured using PROSA II profile analysis.[71-73] The protonation of the final, selected model was done using the Protonate3D module implemented in the Molecular Operating Environment (MOE 2014.09) followed by minimization with a root mean square of 0.5 Å.[74]

3.2 Docking studies

Molecular docking simulations were performed using AutoDock 4.2.[75] The AutoDockTools package was employed to generate docking input files and to analyze the docking results.[75, 76] Docking calculations were performed with full flexibility of the ligand inside the binding site. For each ligand, 50 independent docking calculations using the *var*CPSO-ls algorithm from PSO@Autodock[77] implemented in AutoDock4.2 were performed and terminated after 500,000 evaluation steps. Parameters of the *var*CPSO-ls algorithm, the cognitive and social coefficients c1 and c2, were set to 6.05 with 60 individual particles as a swarm size. Default values were used for all the other available parameters for the grid and docking calculations.

ASSOCIATED CONTENT

AUTHOR INFORMATION

Corresponding Author

*Christa E. Müller: Phone: +49-228-73-230; Fax: +49-228-73-2567; E-mail: christa.mueller@uni-bonn.de

Orcid IDs

Jie Jiang: 0000-0001-5210-6569

Vigneshwaran Namasivayam: 0000-0003-3031-3377

Sonja Hinz: 0000-0001-7942-9536

Christa E. Müller: 0000-0002-0013-6624

Notes

The authors declare no competing financial interest.

ACKNOWLEDGMENT

We thank Nejc Golob and York-Christoph Ammon for contributing to the synthesis of compounds **21** and **23**, respectively. J.J. is grateful to the Alexander von Humboldt Foundation for a post-doctoral fellowship, and J.S. for a DAAD scholarship within the IPID4All program at Bonn University. The authors would like to acknowledge ChemAxon for providing an academic license to their software. This study was supported by the German Federal Ministry of Research and Technology (BMBF) within the BioPharma Neuroallianz consortium (project D11B).

ABBREVIATIONS USED

ADA, adenosine deaminase; AR, adenosine receptor; [^{3}H]CCPA, [^{3}H]2-chloro-N^6-cyclopentyladenosine; CHO cells, Chinese hamster ovary cells; CNS, central nervous system; DIPEA, *N*, *N*-diisopropylethylamine; DCM, dichloromethane; DOPE, discrete optimized protein energy; EDC, *N*-(3-(dimethylamino)propyl)-*N´*-ethylcarbodiimide; ESI, electrospray ionization; GPCR, G protein-coupled receptor; HBSS, Hank's balanced balt bolution; HIF-1α, hypoxia

inducible factor 1-*α*; HEK, human embryonic kidney; HRMS, high-resolution mass spectra; MDSC, myeloid-derived suppressor cells; MOE, Molecular Operating Environment; MS, mass spectrometry; [^{3}H]MSX-2, [^{3}H](*E*)-3-(3-hydroxypropyl)-8-(2-(3-methoxyphenyl)vinyl)-7-methyl-1-prop-2-ynyl-3,7-dihydropurine-2,6-dione; [^{3}H]NECA, [^{3}H]5'-*N*-ethylcarboxamidoadenosine; PET, positron-emission tomography; PPSE, polyphosphoric acid trimethylsilyl ester; PSA, polar surface area; PSB, Pharmaceutical Sciences Bonn; [^{3}H]PSB-603, [^{3}H]8-(4-(4-(4-chlorophenyl)piperazine-1-sulfonyl)phenyl)-1-propyl-3,7-dihydropurine-2,6-dione; [^{3}H]PSB-11, [^{3}H]2-phenyl-8-ethyl-4-methyl-(8*R*)-4,5,7,8-tetrahydro-1*H*-imidazo[2.1-*i*]purin-5-one; RP-HPLC, reverse-phase high performance liquid chromatography; SAR, structure-activity relationships; VTFM, variable target function method.

Supporting Information.

Synthetic procedures for **11** and for the amine building blocks; experimental data for compounds **11**, **13a-c**, **58a**, **58**, **60a-b**, **60**, **62a**, **64a**, **62-64**, **81a**, **81**, **82a**, **82**, **85-87**, **89a**, **89**, **21a**, **41a**; data from cAMP accumulation assays; NMR and LCMS data for selected key compounds; comparison of amino acid sequences of the human AR subtypes; comparison of binding modes of PSB-603 and ZM241385 and possible water-mediated interaction. Molecular formula strings are provided.

Ancillary Information

Authors will release the atomic coordinates of the homology model of the human A_{2B}AR based on the X-ray structure of the human A_{2A}AR (PDB ID 4EIY) upon article publication.

REFERENCES

1. Müller, C. E.; Schiedel, A. C.; Baqi, Y. Allosteric modulators of rhodopsin-like G protein-coupled receptors: Opportunities in drug development. *Pharmacol. Ther.* **2012**, *135*, 292-315.

2. Müller, C. E.; Jacobson, K. A. Recent developments in adenosine receptor ligands and their potential as novel drugs. *Biochim. Biophys. Acta* **2011**, *1808*, 1290-1308.

3. Chen, J.-F.; Eltzschig, H. K.; Fredholm, B. B. Adenosine receptors as drug targets--what are the challenges? *Nat. Rev. Drug Discov.* **2013**, *12*, 265-286.

4. Fredholm, B. B.; IJzerman, A. P.; Jacobson, K. A.; Linden, J.; Müller, C. E. International Union of Basic and Clinical Pharmacology. LXXXI. Nomenclature and classification of adenosine receptors—an update. *Pharmacol. Rev.* **2011**, *63*, 1-34.

5. Fredholm, B. B.; IJzerman, A. P.; Jacobson, K. A.; Klotz, K.-N.; Linden, J. International Union of Pharmacology. XXV. Nomenclature and classification of adenosine receptors. *Pharmacol. Rev.* **2001**, *53*, 527-552.

6. Feoktistov, I.; Biaggioni, I. Adenosine A_{2B} receptors. *Pharmacol. Rev.* **1997**, *49*, 381-402.

7. Vecchio, E. A.; Tan, C. Y. R.; Gregory, K. J.; Christopoulos, A.; White, P. J.; May, L. T. Ligand-independent adenosine A_{2B} receptor constitutive activity as a promoter of prostate cancer cell proliferation. *J. Pharmacol. Exp. Ther.* **2016**, *357*, 36-44.

8. Sommerschild, H. T.; Kirkebøen, K. A. Adenosine and cardioprotection during ischaemia and reperfusion – an overview. *Acta Anaesthesiol. Scand.* **2000**, *44*, 1038-1055.

9. Kong, T.; Westerman, K. A.; Faigle, M.; Eltzschig, H. K.; Colgan, S. P. HIF-dependent induction of adenosine A_{2B} receptor in hypoxia. *FASEB J.* **2006**, *20*, 2242-2250.

10. Ham, J.; Rees, D. A. The adenosine A_{2b} receptor: Its role in inflammation. *Endocr. Metab. Immune.* **2008**, *8*, 244-254.

11. Hinz, S.; Navarro, G.; Borroto Escuela, D.; F. Seibt, B.; Ammon, C.; De Filippo, E.; Danish, A.; K. Lacher, S.; Červinková, B.; Rafehi, M.; Fuxe, K.; Schiedel, A.; Franco, R.; Müller, C.

Adenosine A_{2A} receptor ligand recognition and signaling is blocked by A_{2B} receptors. *Oncotarget* **2018**, *9*, 13593–13611.

12. Jacobson, K. A.; Gao, Z.-G. Adenosine receptors as therapeutic targets. *Nat. Rev. Drug Discov.* **2006**, *5*, 247-264.

13. Müller, C. E.; Baqi, Y.; Hinz, S.; Namasivayam, V. Medicinal Chemistry of A_{2B} Adenosine Receptors. In *The Adenosine Receptors*;Borea, P. A., Varani, K., Gessi, S., Merighi, S., Vincenzi, F., Eds.; Springer International Publishing: Cham, 2018; Vol. 34, pp 137-168.

14. Ryzhov, S.; Novitskiy, S. V.; Zaynagetdinov, R.; Goldstein, A. E.; Carbone, D. P.; Biaggioni, I.; Dikov, M. M.; Feoktistov, I. Host A_{2B} adenosine receptors promote carcinoma growth. *Neoplasia* **2008**, *10*, 987-995.

15. Wei, Q.; Costanzi, S.; Balasubramanian, R.; Gao, Z.-G.; Jacobson, K. A_{2B} adenosine receptor blockade inhibits growth of prostate cancer cells. *Purinergic Signal*. **2013**, *9*, 271-280.

16. Desmet, C. J.; Gallenne, T.; Prieur, A.; Reyal, F.; Visser, N. L.; Wittner, B. S.; Smit, M. A.; Geiger, T. R.; Laoukili, J.; Iskit, S.; Rodenko, B.; Zwart, W.; Evers, B.; Horlings, H.; Ajouaou, A.; Zevenhoven, J.; van Vliet, M.; Ramaswamy, S.; Wessels, L. F. A.; Peeper, D. S. Identification of a pharmacologically tractable Fra-1/$ADORA_{2B}$ axis promoting breast cancer metastasis. *Proc. Natl. Acad. Sci. U.S.A.* **2013**, *110*, 5139-5144.

17. Kasama, H.; Sakamoto, Y.; Kasamatsu, A.; Okamoto, A.; Koyama, T.; Minakawa, Y.; Ogawara, K.; Yokoe, H.; Shiiba, M.; Tanzawa, H.; Uzawa, K. Adenosine A2b receptor promotes progression of human oral cancer. *BMC Cancer* **2015**, *15*, 563.

18. Stagg, J.; Smyth, M. J. Extracellular adenosine triphosphate and adenosine in cancer. *Oncogene* **2010**, *29*, 5346-5358.

19. Antonioli, L.; Blandizzi, C.; Pacher, P.; Hasko, G. Immunity, inflammation and cancer: A leading role for adenosine. *Nat. Rev. Cancer* **2013**, *13*, 842-857.

20. Leone, R. D.; Lo, Y.-C.; Powell, J. D. A2aR antagonists: Next generation checkpoint blockade for cancer immunotherapy. *Comput. Struct. Biotechnol. J.* **2015**, *13*, 265-272.

21. Iannone, R.; Miele, L.; Maiolino, P.; Pinto, A.; Morello, S. Blockade of A_{2b} adenosine receptor reduces tumor growth and immune suppression mediated by myeloid-derived suppressor cells in a mouse model of melanoma. *Neoplasia* **2013**, *15*, 1400-1409.

22. Stagg, J.; Divisekera, U.; McLaughlin, N.; Sharkey, J.; Pommey, S.; Denoyer, D.; Dwyer, K. M.; Smyth, M. J. Anti-CD73 antibody therapy inhibits breast tumor growth and metastasis. *Proc. Natl. Acad. Sci. U.S.A.* **2010**, *107*, 1547-1552.

23. Abo-Salem, O. M.; Hayallah, A. M.; Bilkei-Gorzo, A.; Filipek, B.; Zimmer, A.; Müller, C. E. Antinociceptive effects of novel A_{2B} adenosine receptor antagonists. *J. Pharmacol. Exp. Ther.* **2004**, *308*, 358-366.

24. Eini, H.; Frishman, V.; Yulzari, R.; Kachko, L.; Lewis, E. C.; Chaimovitz, C.; Douvdevani, A. Caffeine promotes anti-tumor immune response during tumor initiation: Involvement of the adenosine A_{2A} receptor. *Biochem. Pharmacol.* **2015**, *98*, 110-118.

25. Merighi, S.; Benini, A.; Mirandola, P.; Gessi, S.; Varani, K.; Simioni, C.; Leung, E.; Maclennan, S.; Baraldi, P. G.; Borea, P. A. Caffeine inhibits adenosine-induced accumulation of hypoxia-inducible factor-1α, vascular endothelial growth factor, and interleukin-8 expression in hypoxic human colon cancer cells. *Mol. Pharmacol.* **2007**, *72*, 395-406.

26. Ohta, A.; Gorelik, E.; Prasad, S. J.; Ronchese, F.; Lukashev, D.; Wong, M. K. K.; Huang, X.; Caldwell, S.; Liu, K.; Smith, P.; Chen, J.-F.; Jackson, E. K.; Apasov, S.; Abrams, S.; Sitkovsky, M. A_{2A} adenosine receptor protects tumors from antitumor T cells. *Proc. Natl. Acad. Sci. U.S.A.* **2006**, *103*, 13132-13137.

27. Dong, S.; Kong, J.; Kong, J.; Shen, Q.; Kong, F.; Sun, W.; Zheng, L. Low concentration of caffeine inhibits the progression of the hepatocellular carcinoma via akt signaling pathway. *Anti-*

Cancer Agents Med. Chem. **2015**, *15*, 484-492.

28. Eastwood, P.; Esteve, C.; González, J.; Fonquerna, S.; Aiguadé, J.; Carranco, I.; Doménech, T.; Aparici, M.; Miralpeix, M.; Albertí, J.; Córdoba, M.; Fernández, R.; Pont, M.; Godessart, N.; Prats, N.; Loza, M. I.; Cadavid, M. I.; Nueda, A.; Vidal, B. Discovery of LAS101057: A potent, selective, and orally efficacious A_{2B} adenosine receptor antagonist. *ACS Med. Chem. Lett.* **2011**, *2*, 213-218.

29. Pastorin, G.; Da Ros, T.; Spalluto, G.; Deflorian, F.; Moro, S.; Cacciari, B.; Baraldi, P. G.; Gessi, S.; Varani, K.; Borea, P. A. Pyrazolo[4,3-e]-1,2,4-triazolo[1,5-c]pyrimidine derivatives as adenosine receptor antagonists. Influence of the N5 substituent on the affinity at the human A_3 and A_{2B} adenosine receptor subtypes: A molecular modeling investigation. *J. Med. Chem.* **2003**, *46*, 4287-4296.

30. El Maatougui, A.; Azuaje, J.; González-Gómez, M.; Miguez, G.; Crespo, A.; Carbajales, C.; Escalante, L.; García-Mera, X.; Gutiérrez-de-Terán, H.; Sotelo, E. Discovery of potent and highly selective A_{2B} adenosine receptor antagonist chemotypes. *J. Med. Chem.* **2016**, *59*, 1967-1983.

31. Taliani, S.; Pugliesi, I.; Barresi, E.; Simorini, F.; Salerno, S.; La Motta, C.; Marini, A. M.; Cosimelli, B.; Cosconati, S.; Di Maro, S.; Marinelli, L.; Daniele, S.; Trincavelli, M. L.; Greco, G.; Novellino, E.; Martini, C.; Da Settimo, F. 3-Aryl-[1,2,4]triazino[4,3-a]benzimidazol-4(10H)-one: A novel template for the design of highly selective A_{2B} adenosine receptor antagonists. *J. Med. Chem.* **2012**, *55*, 1490-1499.

32. Alnouri, M. W.; Jepards, S.; Casari, A.; Schiedel, A. C.; Hinz, S.; Müller, C. E. Selectivity is species-dependent: Characterization of standard agonists and antagonists at human, rat, and mouse adenosine receptors. *Purinergic Signal.* **2015**, *11*, 389-407.

33. Kim, Y.-C.; Ji, X.-d.; Melman, N.; Linden, J.; Jacobson, K. A. Anilide derivatives of an 8-

phenylxanthine carboxylic congener are highly potent and selective antagonists at human A_{2B} adenosine receptors. *J. Med. Chem.* **2000**, *43*, 1165-1172.

34. Kalla, R. V.; Zablocki, J. Progress in the discovery of selective, high affinity A_{2B} adenosine receptor antagonists as clinical candidates. *Purinergic Signal.* **2009**, *5*, 21-29.

35. Baraldi, P. G.; Aghazadeh Tabrizi, M.; Preti, D.; Bovero, A.; Fruttarolo, F.; Romagnoli, R.; Moorman, A. R.; Gessi, S.; Merighi, S.; Varani, K.; Andrea Borea, P. [3H]-MRE 2029-F20, a selective antagonist radioligand for the human A_{2B} adenosine receptors. *Bioorg. Med. Chem. Lett.* **2004**, *14*, 3607-3610.

36. Yan, L.; Müller, C. E. Preparation, properties, reactions, and adenosine receptor affinities of sulfophenylxanthine nitrophenyl esters: Toward the development of sulfonic acid prodrugs with peroral bioavailability. *J. Med. Chem.* **2004**, *47*, 1031-1043.

37. Borrmann, T.; Hinz, S.; Bertarelli, D. C. G.; Li, W.; Florin, N. C.; Scheiff, A. B.; Müller, C. E. 1-Alkyl-8-(piperazine-1-sulfonyl)phenylxanthines: Development and characterization of adenosine A_{2B} receptor antagonists and a new radioligand with subnanomolar affinity and subtype specificity. *J. Med. Chem.* **2009**, *52*, 3994-4006.

38. Chen, M.; Liang, D.; Zuo, A.; Shao, H.; Kaplan, H. J.; Sun, D. An A_{2B} adenosine receptor agonist promotes Th17 autoimmune responses in experimental autoimmune uveitis (EAU) via dendritic cell activation. *PLOS ONE*, **2015**, *10*, e0132348.

39. Du, X.; Ou, X.; Song, T.; Zhang, W.; Cong, F.; Zhang, S.; Xiong, Y. Adenosine A_{2B} receptor stimulates angiogenesis by inducing VEGF and eNOS in human microvascular endothelial cells. *Exp. Bio. Med.* **2015**, *240*, 1472-1479.

40. Ma, D.-F.; Kondo, T.; Nakazawa, T.; Niu, D.-F.; Mochizuki, K.; Kawasaki, T.; Yamane, T.; Katoh, R. Hypoxia-inducible adenosine A_{2B} receptor modulates proliferation of colon carcinoma cells. *Hum. Pathol.* **2010**, *41*, 1550-1557.

41. Karmouty-Quintana, H.; Zhong, H.; Acero, L.; Weng, T.; Melicoff, E.; West, J. D.; Hemnes, A.; Grenz, A.; Eltzschig, H. K.; Blackwell, T. S.; Xia, Y.; Johnston, R. A.; Zeng, D.; Belardinelli, L.; Blackburn, M. R. The A_{2B} adenosine receptor modulates pulmonary hypertension associated with interstitial lung disease. *FASEB J.* **2012**, *26*, 2546-2557.

42. Sun, C.-X.; Zhong, H.; Mohsenin, A.; Morschl, E.; Chunn, J. L.; Molina, J. G.; Belardinelli, L.; Zeng, D.; Blackburn, M. R. Role of A_{2B} adenosine receptor signaling in adenosine-dependent pulmonary inflammation and injury. *J. Clin. Invest.* **2006**, *116*, 2173-2182.

43. Toldo, S.; Zhong, H.; Mezzaroma, E.; Van Tassell, B. W.; Kannan, H.; Zeng, D.; Belardinelli, L.; Voelkel, N. F.; Abbate, A. GS-6201, a selective blocker of the A_{2B} adenosine receptor, attenuates cardiac remodeling after acute myocardial infarction in the mouse. *J. Pharmacol. Exp. Ther.* **2012**, *343*, 587-595.

44. Zhang, H.; Zhong, H.; Everett, T. H.; Wilson, E.; Chang, R.; Zeng, D.; Belardinelli, L.; Olgin, J. E. Blockade of A_{2B} adenosine receptor reduces left ventricular dysfunction and ventricular arrhythmias 1 week after myocardial infarction in the rat model. *Heart Rhythm.* **2014**, *11*, 101-109.

45. Bilkei-Gorzo, A.; Abo-Salem, O. M.; Hayallah, A. M.; Michel, K.; Müller , C. E.; Zimmer, A. Adenosine receptor subtype-selective antagonists in inflammation and hyperalgesia. *Naunyn-Schmiedeberg's Arch. Pharmacol.* **2008**, *377*, 65-76.

46. Hu, X.; Adebiyi, M. G.; Luo, J.; Sun, K.; Le, T.-T. T.; Zhang, Y.; Wu, H.; Zhao, S.; Karmouty-Quintana, H.; Liu, H.; Huang, A.; Wen, Y. E.; Zaika, O. L.; Mamenko, M.; Pochynyuk, O. M.; Kellems, R. E.; Eltzschig, H. K.; Blackburn, M. R.; Walters, E. T.; Huang, D.; Hu, H.; Xia, Y. Sustained elevated adenosine via $ADORA_{2B}$ promotes chronic pain through neuro-immune interaction. *Cell Rep.* **2016**, *16*, 106-119.

47. Yang, Y.; Qiu, Y.; Wang, W.; Xiao, W.; Liang, H.; Zhang, C.; Yang, H.; Teitelbaum, D. H.; Sun, L.-H.; Yang, H. Adenosine A_{2B} receptor modulates intestinal barrier function under hypoxic

and ischemia/reperfusion conditions. *Int. J. Clin. Exp. Pathol.* **2014**, *7*, 2006-2018.

48. Sorrentino, C.; Miele, L.; Porta, A.; Pinto, A.; Morello, S. Myeloid-derived suppressor cells contribute to A_{2B} adenosine receptor-induced VEGF production and angiogenesis in a mouse melanoma model. *Oncotarget* **2015**, *6*, 27478-27489.

49. Kalhan, A.; Gharibi, B.; Vazquez, M.; Jasani, B.; Neal, J.; Kidd, M.; Modlin, I. M.; Pfragner, R.; Rees, D. A.; Ham, J. Adenosine A_{2A} and A_{2B} receptor expression in neuroendocrine tumours: potential targets for therapy. *Purinergic Signal.* **2012**, *8*, 265-274.

50. Figueiredo, A. B.; Souza-Testasicca, M. C.; Mineo, T. W. P.; Afonso, L. C. C. Leishmania amazonensis-induced cAMP triggered by adenosine A_{2B} receptor is important to inhibit dendritic cell activation and evade immune response in infected mice. *Front. Immunol*. **2017**, *8*, 849.

51. Caporarello, N.; Olivieri, M.; Cristaldi, M.; Scalia, M.; Toscano, M. A.; Genovese, C.; Addamo, A.; Salmeri, M.; Lupo, G.; Anfuso, C. D. Blood–brain barrier in a *Haemophilus influenzae* type a in vitro infection: Role of adenosine receptors A_{2A} and A_{2B}. *Mol. Neurobiol.* **2018**, *55*, 5321-5336.

52. Köse, M.; Gollos, S.; Karcz, T.; Fiene, A.; Heisig, F.; Behrenswerth, A.; Kieć-Kononowicz, K.; Namasivayam, V.; Müller, C. E. Fluorescent-labeled selective adenosine A_{2B} receptor antagonist enables competition binding assay by flow cytometry. *J. Med. Chem.* **2018**, *61*, 4301-4316.

53. Sherbiny, F. F.; Schiedel, A. C.; Maaß, A.; Müller, C. E. Homology modelling of the human adenosine A_{2B} receptor based on X-ray structures of bovine rhodopsin, the β2-adrenergic receptor and the human adenosine A_{2A} receptor. *J. Comput. Aided Mol. Des.* **2009**, *23*, 807-828.

54. Thimm, D.; Schiedel, A. C.; Sherbiny, F. F.; Hinz, S.; Hochheiser, K.; Bertarelli, D. C. G.; Maaß, A.; Müller, C. E. Ligand-specific binding and activation of the human adenosine A_{2B} receptor. *Biochemistry* **2013**, *52*, 726-740.

55. Hayallah, A. M.; Sandoval-Ramírez, J.; Reith, U.; Schobert, U.; Preiss, B.; Schumacher, B.; Daly, J. W.; Müller, C. E. 1,8-Disubstituted xanthine derivatives: Synthesis of potent A_{2B}-selective adenosine receptor antagonists. *J. Med. Chem.* **2002**, *45*, 1500-1510.

56. Yan, L.; Yan, D. C. G.; Bertarelli, A.; Hayallah, H.; Meyer, K.-N.; Klotz, C.; Müller. A new synthesis of sulfonamides by aminolysis of p-nitrophenylsulfonates yielding potent and selective adenosine A_{2B} receptor antagonists. *J. Med. Chem.* **2006**, 4*9*, 4384-4391.

57. Priego, E.-M.; Camarasa, M.-J.; Pérez-Pérez, M.-J. Efficient synthesis of N-3-substituted 6-aminouracil derivatives via N6-[(dimethylamino)methylene] protection. *Synthesis* **2001**, *2001*, 0478-0482.

58. Müller, C. E. Synthesis of 3-substituted 6-aminouracils. *Tetrahedron Lett.* **1991**, *32*, 6539-6540.

59. Müller, C. E. General synthesis and properties of 1-monosubstituted xanthines. *Synthesis* **1993**, *1993*, 125-128.

60. Clark, D. E. Rapid calculation of polar molecular surface area and its application to the prediction of transport phenomena. 1. Prediction of intestinal absorption. *J. Pharm. Sci.* **1999**, *88*, 807-814.

61. Lipinski, C. A.; Lombardo, F.; Dominy, B. W.; Feeney, P. J. Experimental and computational approaches to estimate solubility and permeability in drug discovery and development settings. *Adv. Drug Delivery Rev.* **2001**, *46*, 3-26.

62. Petrelli, R.; Scortichini, M.; Kachler, S.; Boccella, S.; Cerchia, C.; Torquati, I.; Del Bello, F.; Salvemini, D.; Novellino, E.; Luongo, L.; Maione, S.; Jacobson, K. A.; Lavecchia, A.; Klotz, K.-N.; Cappellacci, L. Exploring the role of N^6-substituents in potent dual acting 5′-C-ethyltetrazolyladenosine derivatives: Synthesis, binding, functional assays, and antinociceptive effects in mice. *J. Med. Chem.* **2017**, *60*, 4327-4341.

63. Liu, W.; Chun, E.; Thompson, A. A.; Chubukov, P.; Xu, F.; Katritch, V.; Han, G. W.; Roth, C. B.; Heitman, L. H.; IJzerman, A. P.; Cherezov, V.; Stevens, R. C. Structural basis for allosteric regulation of GPCRs by sodium ions. *Science* **2012**, *337*, 232-236.

64. Gao, Z.-G.; Chen, A.; Barak, D.; Kim, S.-K.; Müller, C. E.; Jacobson, K. A. Identification by site-directed mutagenesis of residues involved in ligand recognition and activation of the human A_3 adenosine receptor. *J. Biol. Chem.* **2002**, *277*, 19056-19063.

65. Wilcken, R.; Zimmermann, M. O.; Lange, A.; Joerger, A. C.; Boeckler, F. M. Principles and applications of halogen bonding in medicinal chemistry and chemical biology. *J. Med. Chem.* **2013**, *56*, 1363-1388.

66. Sirimulla, S.; Bailey, J. B.; Vegesna, R.; Narayan, M. Halogen interactions in protein–ligand complexes: Implications of halogen bonding for rational drug design. *J. Chem. Inf. Model.* **2013**, *53*, 2781-2791.

67. Liu, K. G.; Robichaud, A. J. A general and convenient synthesis of N-aryl piperazines. *Tetrahedron Lett.* **2005**, *46*, 7921-7922.

68. Šali, A.; Blundell, T. L. Comparative protein modelling by satisfaction of spatial restraints. *J. Mol. Biol.* **1993**, *234*, 779-815.

69. Shen, M.-y.; Sali, A. Statistical potential for assessment and prediction of protein structures. *Protein Sci.* **2006**, *15*, 2507-2524.

70. Sievers, F.; Wilm, A.; Dineen, D.; Gibson, T. J.; Karplus, K.; Li, W.; Lopez, R.; McWilliam, H.; Remmert, M.; Söding, J.; Thompson, J. D.; Higgins, D. G. Fast, scalable generation of high-quality protein multiple sequence alignments using clustal omega. *Mol. Syst. Biol.* **2011**, *7*, 539.

71. Lovell, S. C.; Davis, I. W.; Arendall, W. B.; de Bakker, P. I. W.; Word, J. M.; Prisant, M. G.; Richardson, J. S.; Richardson, D. C. Structure validation by Cα geometry: ϕ,ψ and Cβ deviation.

Proteins: Struct. Funct. Bioinf. **2003**, *50*, 437-450.

72. Wiederstein, M.; Sippl, M. J. ProSA-web: interactive web service for the recognition of errors in three-dimensional structures of proteins. *Nucleic Acids Res.* **2007**, *35*, W407-W410.

73. Ramachandran, G. N.; Ramakrishnan, C.; Sasisekharan, V. Stereochemistry of polypeptide chain configurations. *J. Mol. Biol.* **1963**, *7*, 95-99.

74. Molecular Operating Environment (MOE 2014.09). In *Chemical Computing Group*, Montreal, Quebec, Canada, 2014.

75. Morris, G. M.; Huey, R.; Lindstrom, W.; Sanner, M. F.; Belew, R. K.; Goodsell, D. S.; Olson, A. J. AutoDock4 and AutoDockTools4: Automated docking with selective receptor flexibility. *J. Comput. Chem.* **2009**, *30*, 2785-2791.

76. Sanner, M. Python: a programming language for software integration and development. *J. Mol. Graph. Model.* **1999**, *17*, 57-61.

77. Namasivayam, V.; Günther, R. Research article: pso@autodock: A fast flexible molecular docking program based on swarm intelligence. *Chem. Biol. Drug Des.* **2007**, *70*, 475-484.

Table of Contents Graphic

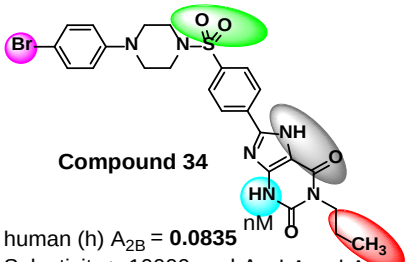

Compound 34

human (h) A_{2B} = **0.0835** nM
Selectivity > 10000 vs. hA_1, hA_{2A}, hA_3
mouse (m) A_{2B} = **0.131** nM
Selectivity > 7600 vs. mA_1, mA_{2A}, mA_3

Most potent A_{2B} adenosine receptor antagonist